

This is an Open Access document downloaded from ORCA, Cardiff University's institutional repository: <https://orca.cardiff.ac.uk/id/eprint/112666/>

This is the author's version of a work that was submitted to / accepted for publication.

Citation for final published version:

Khaki, M., Hamilton, F., Forootan, E. , Hoteit, I., Awange, J. and Kuhn, M. 2018. Non-parametric data assimilation scheme for land hydrological applications. *Water Resources Research* 54 (7) , pp. 4946-4964. 10.1029/2018WR022854

Publishers page: <http://dx.doi.org/10.1029/2018WR022854>

Please note:

Changes made as a result of publishing processes such as copy-editing, formatting and page numbers may not be reflected in this version. For the definitive version of this publication, please refer to the published source. You are advised to consult the publisher's version if you wish to cite this paper.

This version is being made available in accordance with publisher policies. See <http://orca.cf.ac.uk/policies.html> for usage policies. Copyright and moral rights for publications made available in ORCA are retained by the copyright holders.



Non-parametric Data Assimilation Scheme for Land Hydrological Applications

M. Khaki^{a,1}, F. Hamilton^b, E. Forootan^c, I. Hoteit^d, J. Awange^a, M. Kuhn^a

^a*School of Earth and Planetary Sciences, Discipline of Spatial Sciences, Curtin University, Perth, Australia.*

^b*North Carolina State University, Raleigh, North Carolina 27695, USA.*

^c*School of Earth and Ocean Sciences, Cardiff University, Cardiff, UK.*

^d*King Abdullah University of Science and Technology, Thuwal, Saudi Arabia.*

Abstract

1 Data assimilation, which relies on explicit knowledge of dynamical models, is a well-known
2 approach that addresses models' limitations due to various reasons, such as errors in input
3 and forcing datasets. This approach, however, requires intensive computational efforts, es-
4 pecially for high dimensional systems such as distributed hydrological models. Alternatively,
5 data-driven methods offer comparable solutions when the physics underlying the models are
6 unknown. For the first time in a hydrological context, a non-parametric framework is imple-
7 mented here to improve model estimates using available observations. This method uses Takens
8 delay-coordinate method to reconstruct the dynamics of the system within a Kalman filtering
9 framework, called the Kalman-Takens filter. A synthetic experiment is undertaken to fully
10 investigate the capability of the proposed method by comparing its performance with that of a
11 standard assimilation framework based on an adaptive unscented Kalman filter (AUKF). Fur-
12 thermore, using terrestrial water storage (TWS) estimates obtained from the Gravity Recovery
13 And Climate Experiment (GRACE) mission, both filters are applied to a real case scenario
14 to update different water storages over Australia. In-situ groundwater and soil moisture mea-
15 surements within Australia are used to further evaluate the results. The Kalman-Takens filter
16 successfully improves the estimated water storages at levels comparable to the AUKF results,
17 with an average RMSE reduction of 37.30% for groundwater and 12.11% for soil moisture esti-
18 mates. Additionally, the Kalman-Takens filter, while reducing estimation complexities, requires
19 a fraction of the computational time, i.e., ~ 8 times faster compared to the AUKF approach.

Keywords: Non-parametric filtering, Data assimilation, Data-driven, Kalman-Takens, Adaptive unscented Kalman filtering (AUKF), Hydrological modelling.

Email address: Mehdi.Khaki@postgrad.curtin.edu.au (M. Khaki)

20 1. Introduction

21 A precise study of terrestrial water storage (TWS) changes is essential to better un-
22 derstand the spatio-temporal variations of water resources and their effects on the hydrological
23 cycles. In this regard, hydrological models become valuable tools for simulating hydrological
24 processes at global (e.g., [Döll et al., 2003](#); [Huntington, 2006](#); [Coumou and Rahmstorf, 2012](#);
25 [van Dijk et al., 2013](#)) and regional (e.g., [Chiew et al., 1993](#); [Wooldridge and Kalma, 2001](#);
26 [Christiansen et al., 2007](#); [Huang et al., 2016](#)) scales. These models are formulated based on
27 physical/conceptual principles to represent ‘reality’ and are still being developed to accurately
28 simulate all complex hydrological processes, including interactions between water cycle compo-
29 nents (e.g., surface and sub-surface water exchange). These models, however, can be subject to
30 various sources of uncertainties, e.g., errors in input and forcing data, and imperfect accounting
31 for the physical underlying dynamics, such as those used to simulate evapotranspiration ([van](#)
32 [Dijk et al., 2011](#); [Vrugt et al., 2013](#)).

33 Classically, data assimilation can be used to improve imperfect models by integrating avail-
34 able observations with the underlying physical model. Many studies have implemented data
35 assimilation techniques in the fields of ocean and atmospheric sciences (e.g., [Bennett, 2002](#);
36 [Hoteit et al., 2002](#); [Kalnay, 2003](#); [Schunk et al., 2004](#); [Lahoz, 2007](#); [Zhang et al., 2012](#); [Hoteit](#)
37 [et al., 2012](#); [Tardif et al., 2015](#); [Zhao et al., 2017](#)) and hydrology (e.g., [Seo et al., 2003](#); [Vrugt](#)
38 [et al., 2005](#); [Weerts and El Serafy, 2006](#); [Rasmussen et al., 2015](#); [Kumar et al., 2016](#); [Giroto](#)
39 [et al., 2016, 2017](#); [Schumacher et al., 2018](#)). Data assimilation is often used to improve model
40 simulations of soil moisture (e.g., [Entekhabi et al., 1994](#); [Calvet et al., 1998](#); [Montaldo et al.,](#)
41 [2001](#); [Reichle et al., 2002](#); [De Lannoy et al., 2007, 2009](#); [Kumar et al., 2009](#); [Brocca et al., 2010](#);
42 [Renzullo et al., 2014](#); [Kumar et al., 2015](#); [Lievens et al., 2015](#); [De Lannoy et al., 2015](#)), TWS
43 (e.g., [Zaitchik et al., 2008](#); [van Dijk et al., 2014](#); [Tangdamrongsub et al., 2015](#); [Schumacher](#)
44 [et al., 2016, 2018](#); [Khaki et al., 2017a, 2018a,b](#)), evapotranspiration and sensible heat fluxes
45 (e.g., [Schuurmans et al., 2003](#); [Pipunic et al., 2008](#); [Irmak and Kamble, 2009](#); [Yin et al., 2014](#)),
46 surface water and river discharge (e.g., [Bras and Restrepo-Posada, 1980](#); [Awwad et al., 1994](#);
47 [Young, 2002](#); [Madsen and Skotner, 2005](#); [Vrugt et al., 2006](#); [Andreadis et al., 2007](#); [Neal et al.,](#)
48 [2009](#); [Giustarini et al., 2011](#); [Lee et al., 2011](#); [McMillan et al., 2013](#); [Li et al., 2015](#)). Stan-
49 dard data assimilation techniques have their limitations though, e.g., the general requirement
50 of intensive computations for high dimensional systems in realistic applications ([Tandeo et al.,](#)
51 [2015](#)). Furthermore, when a physical model (i.e., model’s underlying equations) is not available,

52 the application of a traditional data assimilation framework that relies on these equations for
53 forecasting can be limited (see, e.g., [Palmer, 2001](#); [Reichle and Koster, 2005](#); [Hersbach et al.,](#)
54 [2007](#); [Arnold et al., 2013](#)).

55 A number of studies employ data-driven (non-parametric) approaches to produce accurate
56 statistical simulations (e.g., [Sauer, 2004](#); [Tandeo et al., 2015](#); [Dreano et al., 2015](#); [Hamilton et](#)
57 [al., 2016](#); [Lguensat et al., 2017](#)). [Hamilton et al. \(2015\)](#) and [Berry and Harlim \(2016\)](#) considered
58 the case when models are partially known. In other cases with completely unknown systems,
59 e.g., no available information about the physics of the underlying models and correspondingly
60 their equations, the application of data assimilation becomes rather complicated. [Hamilton et](#)
61 [al. \(2016\)](#) developed a new model-free filter based on the non-parametric Takens approach and
62 Kalman filtering when the physical model is not available. The main idea of Takens' theorem
63 is that the model equations can be replaced by a data-driven non-parametric reconstruction
64 of the system's dynamics. The filter implements Takens' method for attractor reconstruction
65 within the Kalman filtering framework, allowing for a model-free approach to filter noisy data
66 ([Hamilton et al., 2016](#)). Takens method has been used in various studies for non-parametric
67 time series predictions (see, e.g., [Packard et al., 1980](#); [Takens, 1981](#); [Sauer et al., 1991](#); [Sauer,](#)
68 [2004](#)). This technique replaced the model with a delay coordinate embedding scheme and has
69 been shown by [Hamilton et al. \(2016\)](#) to not only obtain comparable results to a standard
70 Kalman filter-based framework, but also may perform better when model errors are significant.
71 A similar idea has been used by [Tandeo et al. \(2015\)](#) and [Lguensat et al. \(2017\)](#) to simulate the
72 dynamics of complex systems using a non-parametric sampler. They applied an Analog Data
73 Assimilation (AnDA) scheme that reconstructs the system's dynamics in a fully data-driven
74 manner. While AnDA does not require knowledge of the dynamical model, it assumes that a
75 representative catalog of trajectories of the system is available. They show that the data-driven
76 method performs well without using the physical model.

77 The main motivation of this study, therefore, is to apply for the first time the Kalman-
78 Takens method in a hydrological context and investigate its capability to enhance a hydrological
79 model's estimates. Its performance is then compared with that of a traditional data assimilation
80 system. The motivation behind selecting the Kalman-Takens method is that it does not use the
81 model's equations, and requires less computational burden to predict high-dimensional systems
82 compared to other existing methods (e.g., [Hamilton et al., 2015](#); [Tandeo et al., 2015](#); [Berry and](#)
83 [Harlim, 2016](#)). This study extends the Kalman-Takens approach to enable its application to

84 a more complicated state observation transition systems, e.g., for a case of updating various
85 variables (e.g., soil moisture and groundwater) using only TWS observations. The proposed
86 scheme exploits model trajectories for these variables as the training data and is then applied to
87 assimilate TWS data derived from the Gravity Recovery And Climate Experiment (GRACE)
88 satellite mission into the hydrological system states over Australia for the period 2003–2013. It
89 should be pointed out here that the use of model trajectory in this method, and the reliance
90 of data-driven on data in general, results in updating observable state variables only. This,
91 however, is different in a standard data assimilation, which can further update other variables
92 subject to availability of the physical model.

93 GRACE TWS data have been assimilated in many studies, where they have proved to
94 be highly capable of improving the performance of hydrological models (e.g., Zaitchik et al.,
95 2008; van Dijk et al., 2014; Eicker et al., 2014; Reager et al., 2015; Schumacher et al., 2018).
96 Nevertheless, GRACE data assimilation has always been challenging due to the unique charac-
97 teristics of its measurements, such as the coarser spatio-temporal resolution compared to most
98 of the existing hydrological models (Khaki et al., 2017b). A successful data assimilation method
99 should be able to account for these limitations in GRACE products while vertically spreading
100 their information into various water compartments (see, e.g., Schumacher et al., 2016; Khaki
101 et al., 2017b). Khaki et al. (2017a) showed that assimilating GRACE data can significantly
102 improve the hydrological model performance over Australia (see also Khaki et al., 2017c; Tian
103 et al., 2017). In order to benchmark the performance of the proposed data-driven technique, its
104 outputs are compared to those of a standard data assimilation framework based on an adaptive
105 unscented Kalman filter (AUKF, Berry et al., 2013). The results of both methods are evalu-
106 ated against in-situ measurements, as well as through a synthetic experiment to fully investigate
107 their efficiency in assimilating GRACE TWS data.

108 The remainder of this contribution is organized as follow: datasets are presented in Section
109 2, the filtering scheme described in Section 3 and the results discussed in Section 4 before
110 concluding the study in Section 5.

111 2. Model and Data

112 2.1. W3RA

113 The $1^\circ \times 1^\circ$ version of the World-Wide Water Resources Assessment (W3RA;
114 <http://www.wenfo.org/wald/data-software/>) model from the Commonwealth Scientific and In-

115 dustrial Research Organisation (CSIRO) is chosen for the study. The model is designed to
116 simulate landscape water stores and describe the water balance of the soil, groundwater and
117 surface water stores in which each cell is modeled independently of its neighbors (van Dijk, 2010;
118 Renzullo et al., 2014). The model’s forcing includes daily meteorological fields of minimum
119 and maximum temperature, short-wave radiation, and precipitation from Princeton University
120 (Sheffield et al., 2006). The model state vector in our experiment is composed of storages of
121 the top, shallow root and deep root soil layers, groundwater, and surface water for the period
122 of January 2003 to December 2012.

123 2.2. GRACE TWS

124 For the same period, GRACE level 2 (L2) Stokes’ coefficients (up to degree and order
125 90) and associated full error information are obtained from the ITSG-Grace2014 gravity field
126 model (Mayer-Gürr et al., 2014). Three degree 1 coefficients (C10, C11, and S11) and degree 2
127 and order 0 (C20) coefficient are replaced by those of Swenson et al. (2008) and that of Cheng
128 and Tapley (2004), respectively. Further, we apply the DDK2 smoothing filter (Kusche et al.,
129 2009) to mitigate a colored/correlated noise in the coefficients (see also Khaki et al., 2018c), and
130 thereafter convert them into $1^\circ \times 1^\circ$ TWS fields following Wahr et al. (1998). The mean TWS
131 for the study period is taken from the W3RA model and is aggregated to the GRACE TWS
132 change time series to reach absolute values related to W3RA (Zaitchik et al., 2008). Error
133 information of ITSG-Grace2014 is used to construct an observation error covariance matrix
134 (Eicker et al., 2014; Schumacher et al., 2016).

135 2.3. In-situ measurements

136 In-situ groundwater and soil moisture measurements are used to evaluate the perfor-
137 mance of the proposed data assimilation framework. Groundwater data is provided from the
138 New South Wales Government (NSW) within the Murray-Darling Basin, which includes 70%
139 of Australia’s irrigated area, covers an area of over one million square kilometers, and extends
140 over much of the central and south-eastern parts of Australia (Mercer et al., 2007). The data is
141 rescaled to a monthly temporal scale to be consistent with GRACE and time series of ground-
142 water storage anomalies. Considering that a specific yield for converting well-water levels to
143 variations in groundwater storage (Rodell et al., 2007; Zaitchik et al., 2008) is not available, we
144 use the value of 0.13 specific yield obtained from the range between 0.115 and 0.2 as suggested
145 by the Australian Bureau of Meteorology (BOM) and Seoane et al. (2013).

146 Furthermore, in-situ soil moisture products are acquired from the moisture-monitoring net-
147 work, known as the OzNet network (<http://www.oznet.org.au/>), over the Murrumbidgee catch-
148 ment (Smith et al., 2011) and rescaled to the same temporal scale as above. The data contains
149 long-term records of measured volumetric soil moisture at various soil depths at 57 locations
150 across the Murrumbidgee catchment area. Soil measurements at 0–8 cm, the 0–30 cm, and 0–90
151 cm layers are used to assess the estimated soil moisture results of the proposed assimilation
152 framework. The results can be evaluated using representative soil moisture sites within the
153 basin. Here, we use an analysis suggested by De Lannoy et al. (2007) to acquire the represen-
154 tative soil moisture in-situ measurements (see other methods, in e.g., Famiglietti et al., 2008;
155 Orłowsky and Seneviratne, 2014; Nicolai-Shaw et al., 2015). The method is based on relative
156 differences $d_{m,n}$ for site m and time step n , which can be calculated as (De Lannoy et al., 2007),

$$157 \quad d_{m,n} = \frac{SM_{m,n} - \overline{SM}_n}{\overline{SM}_n}, \quad (1)$$

158 where $SM_{m,n}$ is the soil moisture measurement at m and n , and \overline{SM}_n represents the spatially
159 averaged soil moisture. Once $d_{m,n}$ is calculated for each site, the temporally average difference
160 (\bar{d}_m) and its standard deviation ($STD(d_m)$) are computed. The most representative site is then
161 the one with \bar{d}_m and $STD(d_m)$ closer to 0.

162 3. Methodology

163 3.1. Adaptive Unscented Kalman Filter (AUKF)

164 Consider the following nonlinear system,

$$\mathbf{x}_t = \mathbf{f}(\mathbf{x}_{t-1}) + \mathbf{v}_{t-1}, \quad (2)$$

$$\mathbf{y}_t = \mathbf{h}(\mathbf{x}_t) + \mathbf{u}_t, \quad (3)$$

165 where \mathbf{f} , the system dynamics, describes the evolution of state vector, \mathbf{x} , over time (t) and \mathbf{h} ,
166 the observation function, maps \mathbf{x}_t to the observations, \mathbf{y}_t . \mathbf{v}_{t-1} represent the process noise,
167 which is assumed to be Gaussian with mean 0 and covariance \mathbf{Q} . \mathbf{u}_t indicates observation noise
168 with covariance \mathbf{R} , which is assumed to be known (see Section 2). In the present study, \mathbf{x}
169 consists of different water storages including top, shallow and deep soil water, vegetation, snow,
170 surface, and groundwater storages while \mathbf{y} represents the GRACE TWS data.

171 For nonlinear systems, the unscented Kalman filter (UKF) (Julier and Uhlmann, 1997; Julier
 172 et al., 2000; Julier and Uhlmann, 2004; Simon, 2006; Wan and van der Merwe, 2001; Terejanu,
 173 2009) can be used for state estimation. The UKF approximates the propagation of the mean
 174 and covariance of a random variable through a nonlinear function using a deterministic sampling
 175 approach that generates an ensemble of state values known as sigma points. Given the current
 176 state and covariance estimates \mathbf{x}_{t-1}^a and \mathbf{P}_{t-1}^a at step t of the filter, $2L + 1$ sigma points (where
 177 L is the dimension of the state vector) are generated by,

$$\mathbf{x}_{t-1}^0 = \mathbf{x}_{t-1}^a, \quad (4)$$

$$\mathbf{x}_{t-1}^i = \mathbf{x}_{t-1}^a + \left(\sqrt{(L + \lambda)\mathbf{P}_{t-1}^a} \right)_i \quad i = 1, \dots, L, \quad (5)$$

$$\mathbf{x}_{t-1}^{i+L} = \mathbf{x}_{t-1}^a - \left(\sqrt{(L + \lambda)\mathbf{P}_{t-1}^a} \right)_i \quad i = 1, \dots, L, \quad (6)$$

178 with $\left(\sqrt{(L + \lambda)\mathbf{P}_{t-1}^a} \right)_i$ being the i^{th} column of the matrix square root (e.g., lower triangular
 179 Cholesky factorization, Wan and van der Merwe, 2000) of $(L + \lambda)\mathbf{P}_{t-1}^a$. The corresponding
 180 weights to the above sigma points defined as,

$$w_s^0 = \frac{\lambda}{(L + \lambda)}, \quad (7)$$

$$w_c^0 = \frac{\lambda}{(L + \lambda)} + (1 - \alpha^2 + \beta), \quad (8)$$

$$w_s^i = w_c^i = \frac{1}{2(L + \lambda)} \quad i = 1, \dots, 2L, \quad (9)$$

181 where $\sum_{i=0}^{2L} w_s^i = \sum_{i=0}^{2L} w_c^i = 1$. In Eqs. 5–9, λ is the scaling parameter, which can be calculated
 182 as $\lambda = \alpha^2(L + \kappa) - L$. The scaling factor α determines the spread of the sigma points around
 183 \mathbf{x}_{t-1}^a , and κ is a secondary scaling parameter usually set to 0 (the specific value of kappa is not
 184 critical, see e.g., Julier and Uhlmann, 1997; Van der Merwe, 2004). β is employed to incorporate
 185 a prior knowledge about the noise distribution (e.g., the optimal choice for Gaussian distribution
 186 is $\beta = 2$, e.g., Wan and van der Merwe, 2001).

187 Between these factors, the selection of α has larger impacts on the ensemble spreads and
 188 controls the “size” of the sigma-point distribution. α determines how the sigma points can
 189 be scaled towards or away from the mean of the prior distribution. For example, $\alpha = 1$ and
 190 correspondingly $\lambda = 0$ leads the distance between \mathbf{x}_{t-1}^a and the sigma points to be proportional
 191 to \sqrt{L} . Positive values of λ (for $\alpha > 1$) scales the sigma points further from \mathbf{x}_{t-1}^a while negative

192 values of λ (for $\alpha < 1$) scales the sigma points towards \mathbf{x}_{t-1}^a . In other words, the larger values
 193 for this scaling factor causes a larger spread in the sigma points while smaller values result in
 194 more concentration around prior distribution (Van der Merwe, 2004). Ideally α should be a
 195 small number, e.g., $1e - 4 \leq \alpha \leq 1$ (Song and He, 2005) to avoid sampling non-local effects
 196 when the nonlinearities are strong. However, optimal sets of this factor along with κ and β are
 197 generally problem specific and can be optimized arbitrary. For the current study, the values
 198 of parameters are assumed as $\alpha = 0.5$, $\kappa = 0$, and $\beta = 2$. Nevertheless, it is found that the
 199 implemented AUKF is not very sensitive to the parameter selection as long as they result in a
 200 numerically well-behaved set of sigma-points and weights (see also Van der Merwe, 2004).

201 The sigma points are advanced forward one time step using model \mathbf{f} and observed using the
 202 function \mathbf{h} ,

$$\mathbf{x}_t^{f,j} = \mathbf{f}(\mathbf{x}_{t-1}^j), \quad \mathbf{j} = \mathbf{0}, \dots, \mathbf{2L}, \quad (10)$$

$$\mathbf{y}_t^{f,j} = \mathbf{h}(\mathbf{x}_t^{f,j}), \quad \mathbf{j} = \mathbf{0}, \dots, \mathbf{2L}. \quad (11)$$

203 The transformed points ($\mathbf{x}_t^{f,j}$ and $\mathbf{y}_t^{f,j}$) are then used to calculate their respective forecast means
 204 and covariance matrices,

$$\mathbf{x}_t^f = \sum_{j=0}^{2L} w_s^j \mathbf{x}_t^{f,j}, \quad (12)$$

$$\mathbf{y}_t^f = \sum_{j=0}^{2L} w_s^j \mathbf{y}_t^{f,j}, \quad (13)$$

$$\mathbf{P}_t^f = \sum_{j=0}^{2L} w_c^j (\mathbf{x}_t^{f,j} - \mathbf{x}_t^f) (\mathbf{x}_t^{f,j} - \mathbf{x}_t^f)^T + \mathbf{Q}_{t-1}, \quad (14)$$

$$\mathbf{P}_{\mathbf{y}_t^f} = \sum_{j=0}^{2L} w_c^j (\mathbf{y}_t^{f,j} - \mathbf{y}_t^f) (\mathbf{y}_t^{f,j} - \mathbf{y}_t^f)^T + \mathbf{R}_t, \quad (15)$$

205 as well as the cross covariance between \mathbf{x}_t^f and \mathbf{y}_t^f ,

$$\mathbf{P}_{\mathbf{x}_t^f, \mathbf{y}_t^f} = \sum_{j=0}^{2L} w_c^j (\mathbf{x}_t^{f,j} - \mathbf{x}_t^f) (\mathbf{y}_t^{f,j} - \mathbf{y}_t^f)^T. \quad (16)$$

206 In the analysis step of the filter, the measurements (e.g., GRACE-derived TWS) are used
 207 to correct the forecasted state and respective covariance matrix using the Kalman update

208 equations,

$$\mathbf{x}_t^a = \mathbf{x}_t^f + \mathbf{K}(\mathbf{y}_t - \mathbf{y}_t^f), \quad (17)$$

$$\mathbf{K} = \mathbf{P}_{\mathbf{x}_t^f, \mathbf{y}_t^f} \mathbf{P}_{\mathbf{y}_t^f}^{-1}, \quad (18)$$

$$\mathbf{P}_t^a = \mathbf{P}_{\mathbf{x}_t^f} - \mathbf{K} \mathbf{P}_{\mathbf{y}_t^f} \mathbf{K}^T. \quad (19)$$

209 where \mathbf{K} is the Kalman gain.

210 Critical to the success of the UKF is the selection of the filter noise covariances, and in
 211 particular the process noise covariance matrix \mathbf{Q} . Here, we use the method of [Berry et al.](#)
 212 (2013) to adaptively estimate this covariance matrix. We refer to this as the *adaptive unscented*
 213 *Kalman filter* (AUKF). Building on the method of [Mehra \(1990, 1992\)](#), the general idea of [Berry](#)
 214 [et al. \(2013\)](#) is to use the increment, $\epsilon_t = \mathbf{y}_t - \mathbf{y}_t^f$, to estimate the noise covariance at each time
 215 step. The method begins by forming an empirical estimate \mathbf{Q}_{t-1}^e for \mathbf{Q} ,

$$\mathbf{P}_{t-1}^e = \mathbf{F}_{t-1}^{-1} \mathbf{H}_{t-1}^{-1} \epsilon_{t-1} \epsilon_{t-1}^T \mathbf{H}_{t-1}^{-T} + \mathbf{K}_{t-1} \epsilon_{t-1} \epsilon_{t-1}^T \mathbf{H}_{t-1}^{-T}, \quad (20)$$

$$\mathbf{Q}_{t-1}^e = \mathbf{P}_{t-1}^e - \mathbf{F}_{t-2} \mathbf{P}_{t-2}^a \mathbf{F}_{t-2}^T, \quad (21)$$

216 where \mathbf{P}_{t-1}^e is an empirical estimate of the background covariance. In Eqs. 20 and 21, \mathbf{F}
 217 and \mathbf{H} are local linearizations of the nonlinear dynamic models \mathbf{f} and \mathbf{h} , respectively, and are
 218 estimated using a linear regression on the ensembles (see Eq. 7 in [Berry et al., 2013](#), for
 219 details regarding this linearization). It is worth mentioning that we must store linearizations
 220 $\mathbf{F}_{t-2}, \mathbf{F}_{t-1}, \mathbf{H}_{t-1}, \mathbf{H}_t$, increments $\epsilon_{t-1}, \epsilon_t$, analysis covariance \mathbf{P}_{t-2}^a , and Kalman gain \mathbf{K}_{t-1} from
 221 the $t-1$ and $t-2$ steps of the filter. To form a stable estimate of \mathbf{Q} , the noisy estimate \mathbf{Q}_{t-1}^e
 222 is combined using an exponentially weighted moving average,

$$\mathbf{Q}_t = \mathbf{Q}_{t-1} + (\mathbf{Q}_{t-1}^e - \mathbf{Q}_{t-1})/\tau, \quad (22)$$

223 where τ is the window of the moving average. [Berry et al. \(2013\)](#); [Hamilton et al. \(2016\)](#) provide
 224 additional details on the estimation of noise covariance.

225 3.2. Kalman-Takens Method

226 The main idea of the Kalman-Takens method is to replace the model-based forecast in the
 227 AUKF with the advancement of the dynamics non-parametrically, thus requiring no knowledge

228 of \mathbf{f} (in Eq. 2). We provide a brief description of the method below, specifically highlighting
 229 modifications in adopting the algorithm to our problem. Full details of the methodology can
 230 be found in [Hamilton et al. \(2016, 2017\)](#).

231 In the present study, we consider a different setup to implement the Kalman-Takens filter for
 232 a more complicated state observation transition systems. While the data available are gridded
 233 GRACE TWS, our interest is in estimating the different water variables (i.e., top, shallow
 234 and deep soil water, vegetation, snow, surface, and groundwater). These variables with no
 235 independent observation available, are provided by the W3RA model and are used to produce
 236 delay-coordinate vectors. We generate a synthetic set of model trajectories (open-loop run) for
 237 these variables to serve as the training data for the Kalman-Takens filter. The training data
 238 represents the state of the system. It is also used to generate a local proxy $\tilde{\mathbf{f}}$ for the unknown
 239 model \mathbf{f} (cf. Eq. 2), which is not available in the non-parametric framework, so Eq. 10 for
 240 advancing the ensemble forward in time in AUKF is not implementable. This brings us to Eq.
 241 23, which defines the delay-coordinate vector \mathbf{z} at each step of the filter using the historical
 242 state variables from the open-loop run by,

$$\mathbf{z}_t = [\mathbf{x}_t^{\mathbf{o}}, \mathbf{x}_{t-1}^{\mathbf{o}}, \dots, \mathbf{x}_{t-d}^{\mathbf{o}}], \quad (23)$$

243 where d is the number of temporal delays. $\mathbf{x}^{\mathbf{o}}$ contains the open-loop top, shallow and deep soil
 244 moisture, vegetation, snow, surface, and groundwater. Once the delay coordinate is created,
 245 the assimilation procedure can be applied. At each AUKF step, an ensemble of delay vectors
 246 is formed and advanced non-parametrically using a local approximation $\tilde{\mathbf{f}}$. This nonparametric
 247 prediction helps to build local models for predicting the dynamics at the forecast step ([Hamilton
 248 et al., 2017](#)). Given the above current delay-coordinate, the non-parametric advancement starts
 249 by locating the N nearest neighbors (i.e., points located within a given Euclidean distance; not
 250 only adjacent points), within a set of training data,

$$\begin{aligned} \mathbf{z}_t^1 &= [\mathbf{x}_t^{\mathbf{o}1}, \mathbf{x}_{t-1}^{\mathbf{o}1}, \dots, \mathbf{x}_{t-d}^{\mathbf{o}1}], \\ \mathbf{z}_t^2 &= [\mathbf{x}_t^{\mathbf{o}2}, \mathbf{x}_{t-1}^{\mathbf{o}2}, \dots, \mathbf{x}_{t-d}^{\mathbf{o}2}], \\ &\vdots \\ \mathbf{z}_t^N &= [\mathbf{x}_t^{\mathbf{o}N}, \mathbf{x}_{t-1}^{\mathbf{o}N}, \dots, \mathbf{x}_{t-d}^{\mathbf{o}N}]. \end{aligned} \quad (24)$$

251 The known $\mathbf{z}_{t+1}^1, \mathbf{z}_{t+1}^2, \dots, \mathbf{z}_{t+1}^N$ (based on $\mathbf{x}_{t+1}^{o1}, \mathbf{x}_{t+1}^{o2}, \dots, \mathbf{x}_{t+1}^{oN}$), are used in a local model to
 252 predict \mathbf{z}_{t+1} . The local model $\tilde{\mathbf{f}}$, which can be generated using a weighted average of the nearest
 253 neighbors (Hamilton et al., 2016; Lagergren et al., 2018) can be written as,

$$\mathbf{z}_{t+1} = \omega_1 \mathbf{z}_{t+1}^1 + \omega_2 \mathbf{z}_{t+1}^2 + \dots + \omega_N \mathbf{z}_{t+1}^N, \quad (25)$$

$$\omega_i = \frac{e^{-(d_i/\sigma)^2}}{\sum_{j=1}^N e^{-(d_j/\sigma)^2}}, \quad (26)$$

254 where d_i is the distance of the j^{th} neighbour to \mathbf{z}_t and σ is a bandwidth parameter, which
 255 controls the contribution of each neighbor in the local model (here $\sigma = 2$). The above prediction
 256 is applied to estimate the delay coordinate vector at $t + 1$.

257 The process of building a local model for forecasting the delay-coordinate vector is repeated
 258 for each sigma point in the ensemble. After $\tilde{\mathbf{f}}$ has been defined, the remainder of the AUKF
 259 update scheme is implemented. Important to the Kalman-Takens method is the selection of d
 260 (the number of delays) and neighbors N . Here, we consider different values of N and d and
 261 set them based on the filter performance, which is described in Section 4. The assumption of
 262 using the model trajectory rather than observations for generating delay vectors allows us to
 263 reconstruct the system representing various water storage compartments. The same assumption
 264 is made by Lguensat et al. (2017), where trajectories of the system and not the physical model
 265 is available. In fact, we hypothesize that the available model outcomes can be used for the
 266 non-parametric sampling of the dynamics and updated by the GRACE TWS (as a summation
 267 of all the water variables at each grid point). This means that one can essentially correct
 268 state variables of the system, without having data for each individually, using the data-driven
 269 framework. The application of this method can address some severe limitations in traditional
 270 data assimilation such as large computational cost.

FIGURE 1

271 3.3. Synthetic experiment

272 A synthetic experiment is undertaken to assess the efficiency of the proposed data as-
 273 simulation schemes in simulating physical processes. One important problem with hydrological
 274 models, and specifically W3RA, is their limitations in simulating anthropogenic impacts on
 275 the water cycle. For example, excessive groundwater extractions, which can largely affect sub-

276 surface water storages, are not modeled in W3RA and a successful data assimilation process
 277 should be able to correct for this drawback by taking the advantage of additional observations.
 278 Here, we choose to test both AUKF and Kalman-Takens filters to improve upon model simula-
 279 tions between 2003 and 2013 over Iran ($32.4279^\circ N$, $53.6880^\circ E$). The rationale behind choosing
 280 Iran for this synthetic analysis, and not Australia, is that a remarkable water storage decline
 281 is reported over this region, mainly due to anthropogenic impacts, which cannot be detected
 282 by W3RA (see [Khaki et al., 2018b](#)). A major part of the negative water storage trend is due
 283 to human impacts (see details in [Forootan et al., 2017](#); [Khaki et al., 2018b](#)). Synthetic ob-
 284 servations are produced using the WaterGAP Global Hydrology Model (WGHM; [Döll et al.,](#)
 285 [2003](#); [Müller et al., 2014](#)) monthly TWS outputs, which contain the anthropogenic impacts
 286 ([Khaki et al., 2018b](#)), at two different spatial resolution of $1^\circ \times 1^\circ$ and $3^\circ \times 3^\circ$. This can help
 287 to test whether data assimilation can account for human impacts on water storage and also
 288 to investigate the effect of spatial resolution on the final results. WGHM TWS estimates are
 289 assumed as our observations after rescaling into $1^\circ \times 1^\circ$ and $3^\circ \times 3^\circ$ and perturbing using Monte
 290 Carlo sampling of multivariate normal distributions with the errors representing the GRACE
 291 level 2's standard errors. The data assimilation is implemented using both filtering methods at
 292 the aforementioned spatial scales.

293 3.4. Evaluation metrics

294 To evaluate the assimilation results against in-situ groundwater and soil moisture mea-
 295 surements, three metrics, (i) the Root-Mean-Squared Errors (RMSE), (ii) standard deviation
 296 (STD), and (iii) Nash-Sutcliffe coefficient (NSE) are used. Groundwater and soil moisture in-
 297 situ measurements from various stations are spatially averaged to the location of the nearest
 298 model grid points and are compared with their respective estimates. To this end, using the
 299 variation time series of in-situ data and the results of assimilation techniques, RMSE, STD,
 300 and NSE are calculated by,

$$RMSE = \sqrt{\frac{1}{n} \sum_{i=1}^n (x_i - z_i)^2}, \quad (27)$$

$$STD = \sqrt{\frac{1}{n} \sum_{i=1}^n (x_i - \bar{x})^2}, \quad (28)$$

$$NSE = 1 - \left[\frac{\sum_{i=1}^n (x_i - z_i)^2}{\sum_{i=1}^n (z_i - \bar{z})^2} \right], \quad (29)$$

301 where x_i is the predicted value (for n samples) and z_i represents the measured in-situ value.
302 In Eqs. 27–29, \bar{x} and \bar{z} are the average of the predicted and measured values, respectively.
303 Furthermore, to statistically assess the significance of the results, the student t-test is applied.
304 The estimated t-value and the distribution at 0.05 significant level are used to calculate p-values.

305 4. Results

306 4.1. Synthetic experiment

307 The results of synthetic experiment, which is chosen to assess the capability of the two
308 data assimilation schemes in improving model’s simulation of physical processes are presented in
309 this section. TWS variations from W3RA (open-loop; model integration without assimilation),
310 AUKF and Kalman-Takens filters (with $N = 14$ and $d = 11$, see Section 4.2 for details), as well
311 as synthetic observations, are displayed in Figure 2, where the time series represent spatially
312 averaged TWS variations over the entire Iran. The trend lines corresponding to each time series
313 are also depicted in the figure. As can be clearly seen, W3RA’s open-loop run does not correctly
314 capture the negative trend in the TWS time series as visible in the observations. Assimilation
315 results, on the other hand, successfully reproduce the negative trend. Except for few cases,
316 e.g., 2009 and 2011, Kalman-Takens performs closely to AUKF. The assimilation trend lines
317 also show that the filtered results capture the existing trend of the observations. In addition to
318 the trends, there are larger correlations between AUKF (14% on average) and Kalman-Takens
319 (12% on average) with the observations compared to the open-loop results. An evaluation of the
320 assimilation results against the original WGHM TWS, i.e., before perturbation using GRACE
321 noises, are shown in Figure 3.

FIGURE 2

322 Figure 3 shows the scatter plot of the open-loop, AUKF, and Kalman-Takens TWS esti-
323 mates against WGHM at the two spatial resolutions of $1^\circ \times 1^\circ$ and $3^\circ \times 3^\circ$ to assess the filters’
324 performances at various spatial scales. Note that temporal assessment is also investigated in
325 Section 4.2. It can be seen that at both spatial scales, there are larger agreements between the
326 filtered results and WGHM. There are also smaller RMSEs after filtering, which suggests the
327 capability of both methods to improve model simulations even in case of remarkable human
328 impact. While every assimilation scenario leads to smaller RMSE than the open-loop run, the

329 least RMSEs are achieved at $1^\circ \times 1^\circ$ resolution. This shows that assimilating TWS observations
330 at a finer resolution can provide better estimates regardless of the filtering method. It can also
331 be seen that both AUKF and Kalman-Takens provide comparable results at both spatial scales,
332 leading to approximately 48% RMSE reduction. The filters' comparable results at $3^\circ \times 3^\circ$ spa-
333 tial resolution suggests their similar performance for downscaling TWS observations into the
334 $1^\circ \times 1^\circ$ W3RA resolution.

FIGURE 3

335 4.2. Assessment with in-situ data

336 Independent groundwater and soil moisture in-situ measurements within the Murray-
337 Darling Basin in Australia are used to evaluate the results. This is done by comparing the
338 AUKF and Kalman-Takens estimates of groundwater and soil moisture with those of the in-
339 situ measurements. Note that further analysis is undertaken to assess the impacts of the filters
340 on non-assimilated variables and the results are provided in the supplementary material. Before
341 comparing AUKF and Kalman-Takens results against in-situ measurements, we investigate the
342 effect of various setups in the Kalman-Takens performance. Different scenarios are considered
343 regarding the number of neighbors N (i.e., 2–40) and also the number of delays d (i.e., 1–25).
344 To reach the best setup amongst these values, we compare the results of each scenario to the
345 in-situ groundwater measurements. Figure 4 shows the average absolute groundwater errors
346 resulting from each case. Increasing the number of neighbors can improve the approximation of
347 training data for a particular point to a certain extent (due to the existing spatial correlations).
348 However, selecting N too large can cause a rapid growth of errors, which is related to the effect
349 of over-smoothing the training step. This is different for delays d , where much larger errors
350 are present for smaller values that underestimate temporal variabilities in the data. From our
351 numerical investigations, it can be seen that applying the Kalman-Takens filter with $N = 14$
352 and $d = 11$ provides the best result. It is worth mentioning that we use these setups of the
353 Kalman-Takens filter throughout this study.

FIGURE 4

354 The comparison between the open-loop run, AUKF, and Kalman-Takens results are de-
355 picted in Figure 5, which displays scatter plot of each filter's RMSE and STD calculated using

356 in-situ groundwater measurements. Three different temporal evaluations are considered to fur-
357 ther investigate the effect of temporal downscaling on the results. The GRACE TWS data
358 (with approximately 30 days temporal scale) and associated errors are interpolated into a daily
359 and 5-daily samples (see also [Tangdamrongsub et al., 2015](#); [Khaki et al., 2017b](#)) using the
360 spline interpolation between consecutive months. The assimilation is then undertaken on a
361 daily, 5-day, and monthly basis. Figure 5 indicates that both AUKF and Kalman-Takens filters
362 result in smaller RMSE and STD compared to the open-loop run for all the three temporal
363 scales. In the daily and to a lesser degree 5-day assimilation cases, AUKF performs slightly
364 better than the Kalman-Takens, with smaller RMSE and STD, which could be attributed to the
365 contribution of the model equations for spreading TWS information between different variables
366 after assimilation. Nevertheless, the performance of the non-parametric filter is satisfactory for
367 both cases and comparable to that of AUKF. Interestingly, the performances of the two filters
368 are even closer when assimilating monthly data. As a general result, this demonstrates that
369 temporal downscaling of GRACE TWS data is recommended for data assimilation purpose
370 regardless of the filtering method used. The average RMSE values for the 5-day assimilation
371 using AUKF and Kalman-Takens filters are 51.28 ($\sim 13\%$ smaller than daily and $\sim 7\%$ smaller
372 than monthly) and 53.61 ($\sim 16\%$ smaller than daily and $\sim 5\%$ smaller than monthly), respec-
373 tively. Based on the above evaluation, it can be concluded that different temporal scales have
374 similar effects on both filters, where the AUKF and Kalman-Takens filters perform better for
375 the 5-day assimilation case.

FIGURE 5

376 More detailed statistics are provided in Table 1 to better compare the performances of the
377 implemented filters against in-situ groundwater measurements. The evaluation is undertaken
378 using RMSE and NSE metrics (see Section 3.4) based on the 5-day assimilation case. Note
379 that in this table, basin-scale results are provided in addition to the results of the grid-based
380 evaluation. Considering the coarse spatial resolution of W3RA and the fact that a number of
381 groundwater stations can be found in each grid cell, basin-averaged assessment is performed as
382 an alternative examination. The spatially averaged open-loop results and those from filters over
383 the Murray-Darling Basin are tested against basin-average groundwater time series. Results of
384 Table 1 confirm the behavior seen in Figure 5. While smaller RMSEs are obtained from AUKF

385 for both grid- and basin-based tests, the application of the Kalman-Takens method significantly
386 decreases groundwater RMSE values (30.22% on average). Also larger NSE values are obtained
387 by both filters compared to the open-loop run. These results prove a high capability of the
388 Kalman-Takens for improving state estimates, very close to the AUKF performance. Table 1
389 also indicates that the Kalman-Takens approach can be used as traditional data assimilation
390 to reduce noise in the final state variables, which are the results of solving complex inverse
391 problems, e.g., groundwater estimates are improved from GRACE-derived TWS. This is also
392 true for soil moisture estimates (cf. Table 2).

TABLE 1

393 We use different soil moisture layers from in-situ measurements including 0-8 cm (compared
394 to the model top soil moisture layer), 0-30 cm (compared to the summation of the model top
395 and shallow soil moisture layers), and 0-90 cm (compared to the summation of the model top,
396 shallow, and deep soil moisture layers) for evaluating the results. Note that considering the
397 difference between W3RA states (i.e., column water storage measured in mm) and the OzNet
398 measurements (i.e., volumetric soil moisture) and the fact that converting the model outputs
399 into volumetric units may introduce a bias (Renzullo et al., 2014), only NSE analysis is carried
400 out and the results are provided in Table 2. Similar improvements as for groundwater evaluation
401 are also found by comparing the filters estimates against OzNet soil moisture measurements
402 (Table 2). Larger NSE values are found from data assimilation filters for all three soil layers.
403 Average NSE from the Kalman-Takens method is 0.73, $\sim 12.3\%$ larger than the open-loop run,
404 and slightly smaller than AUKF results (0.74). Table 2 confirms that the capability of the
405 Kalman-Takens method for improving the soil moisture estimates similar to AUKF (13.7% on
406 average). The largest improvements for both filters are achieved in the root zone (0–90 cm)
407 moisture layer. Table 2 suggests that AUKF better reflects the GRACE observations, especially
408 at this layer. This, however, does not necessarily lead to better approximations in the shallow
409 soil moisture layer, where the non-parametric approach shows higher improvements compared
410 to AUKF.

TABLE 2

411 *4.3. Assessing the performance of AUKF and Kalman-Taken filters*

412 Here, we compare the performances of the AUKF and Kalman-Takens filters from various
413 perspectives including increment applied, state covariance, computational efficiency, and water
414 storage forecasting. Figure 6 shows the increments implemented by each filtering technique
415 during the study period. We estimate average increment (i.e., ϵ discussed in Section 3.1) at
416 all grid points for AUKF and the Kalman-Takens approach. One can see how the filters deal
417 with the GRACE TWS observations in the update steps. Both methods decrease the increment
418 as assimilation proceeds forward in time. This is found to be smaller for the Kalman-Takens
419 method (see the trend lines in Figure 6) compared to AUKF. In fact, AUKF integrates the
420 ensemble members through the model \mathbf{f} , while the non-parametric approach uses the local
421 proxy $\tilde{\mathbf{f}}$. Consequently, larger misfits between the Kalman-Takens method forecast estimates
422 and observations can be expected. Nevertheless, Figure 6 shows that the local proxy performs
423 comparably to \mathbf{f} in most of the time. In addition to increments, the difference between the
424 filter's forecasting also affects the estimated error covariances, especially forecast covariance
425 matrix (cf. Figure 7).

426 FIGURE 6

FIGURE 7

427 P_f and P_a are calculated at assimilation steps for both filters. The average of the matrices'
428 diagonal elements are displayed in Figure 7. Despite the filters different performances in Figure
429 6, both methods perform very similar in dealing with the error covariances. The distribution of
430 scattered error points from the Kalman-Takens filter and the corresponding trend line largely
431 matches that of AUKF, which demonstrate that the filters have comparable uncertainty esti-
432 mates. This indicates the ability of the Kalman-Takens method, which not only improves the
433 model states but is also competitive with the traditional data assimilation system.

434 *4.3.1. Filters efficiency*

435 Computational complexity is important for data assimilation methods, especially when
436 dealing with a high dimensional system, such as in hydrological studies. Therefore, a good data
437 assimilation filter requires balancing between processes undertaken to achieve accurate estimates
438 and computational efficiency. While the Kalman-Takens filter's capability for improving state

439 estimates have already been demonstrated (cf. Sections 4.1 and 4.2), its potential for decreasing
440 the computational cost is examined here. This is done by comparing the computation time of the
441 AUKF and Kalman-Takens filtering methods from various perspectives including forecasting,
442 analysis steps, and filtering over the entire study period. Importantly, the following computation
443 time estimates have been obtained using identical hardware. In the forecast step, the average
444 computation time (for 794 grid points within Australia) is considerably lower for the Kalman-
445 Takens filter, e.g., 6.12 second against 8.57 second for AUKF. This is due to the fact that the
446 Kalman-Takens filter exploits the proxy model (\tilde{f}), which is based on a local approximation and
447 requires much less computation than a physics-based model. The average computational time
448 at the analysis steps is 5.74 second for the Kalman-Takens filter and 7.83 seconds for AUKF.
449 Considering that both methods are using similar analysis filtering, this difference is due to the
450 local scheme (based on d delays and N neighbor points) in the Kalman-Takens method. The
451 values of delays d and neighbors N determine the number of local points used in the analysis
452 and accordingly the size of the underlying vectors and matrices. AUKF, on the other hand,
453 solves for all grid points altogether, which requires a larger amount of memory and time. In
454 general, it is found that the Kalman-Takens is considerably less computationally demanding,
455 i.e., ~ 8 times faster for the entire experiment period, compared to the AUKF implementation
456 for assimilating all observations into the system states.

457 4.3.2. Water storage update

458 In this section, we analyze the spatio-temporal increments derived by assimilating the
459 GRACE TWS observations and explore their effects on the states. Figure 8 presents the average
460 TWS time series after applying each filter, open-loop, and GRACE observations over Australia.
461 Both filters largely decrease the misfits between the model states and the GRACE observations,
462 which is expected since GRACE is used as a constraint. AUKF, however, has a larger impact
463 on the states, especially where a significant TWS variation exists (e.g., 2006 and 2011–2012).
464 The Kalman-Takens method, on the other hand, shows a smoother time series. Based on these
465 results, we find that the Kalman-Takens approach is able to efficiently integrate observations
466 into the model and correct missing trends as well as amplitudes and phases. Nevertheless, one
467 can conclude that this method might not be able to efficiently extract spontaneous or high rate
468 seasonal effects unless the training data has these variabilities/dynamics.

FIGURE 8

469 The correlation between the estimated TWS time series from the open-loop model run
470 and the filters' estimates at each grid point within Australia and those of the GRACE TWS
471 are presented in Figure 9. The filters largely increase the correlation between model derived
472 TWS and those of GRACE. The largest correlations (with 0.92 average) is obtained by AUKF
473 suggesting that this method better reflects the GRACE TWS into the states. The average
474 correlation between TWS of the Kalman-Takens and GRACE is 0.89 (0.03 less than AUKF),
475 and when compared to only 0.52 obtained from the open-loop estimates, the efficiency of the
476 method becomes visible. Correlations of the open-loop TWS and GRACE are smaller over the
477 mountainous area along the East coast compared to other parts of the country. This is due to
478 difficulties of modeling hydrology in complex terrain areas (mountains). On the other hand,
479 both assimilation methods show good performances by increased correlations with GRACE
480 data. Over large parts of Australia, the performances of the Kalman-Takens filter and AUKF
481 are found to be similar in terms of correlations with the GRACE TWS.

FIGURE 9

482 To further assess the capability of the filtering approaches for improving the model simu-
483 lations, we test their ability in correcting the model variables for extreme and poorly known
484 hydrological phenomena. To this end, the filters' TWS results are monitored between 2003
485 and 2012 over the Murray-Darling Basin. As shown by [Schumacher et al. \(2018\)](#), a long-term
486 drought period (2001–2009), known as Millennium Drought (e.g., [Ummenhofer et al., 2009](#);
487 [LeBlanc et al., 2012](#); [van Dijk et al., 2013](#)), has remarkably affected TWS variations in the
488 basin. This negative TWS trend has then been followed by an above average precipitation,
489 mainly caused by El Niño Southern Oscillation (ENSO; see, e.g., [Boening et al., 2012](#); [Forootan
490 et al., 2016](#)) for the period of 2010–2012. Here, we investigate the capability of the open-loop,
491 AUKF, and Kalman-Takens TWS estimates to capture these two extreme events. Figure 10
492 plots the average TWS time series of the above methods, as well as GRACE-derived TWS over
493 the Murray-Darling Basin. As can be seen, while both Millennium drought (red shaded area)
494 and ENSO effect (blue shaded area) are reflected in GRACE TWS time series, the open-loop
495 run is unable to capture them, especially the drought effects. AUKF and the Kalman-Takens

496 filter, on the other hand, successfully depict the negative trend between 2003 and 2010, fol-
497 lowed by a positive anomaly after 2010. Except for few points such as 2004, 2007, and late
498 2009, the Kalman-Takens method presents a similar performance as AUKF in incorporating
499 GRACE TWS data with states and reflecting extreme hydrological events.

FIGURE 10

500 5. Conclusions

501 The present study investigates the ability of the Kalman-Takens approach to reconstruct
502 the nonlinear dynamics of a hydrological model. This is done to update observable state vari-
503 ables based on new observations when a physics-based model is not available. This implies that
504 contrary to a standard data assimilation, the Kalman-Takens filter does not affect non-observed
505 variables (e.g., water discharge in our case). In this work, we introduce a new setup for the
506 Kalman-Takens filter to reconstruct additional states (e.g., soil moisture and groundwater) us-
507 ing the Gravity Recovery And Climate Experiment (GRACE) terrestrial water storage (TWS).
508 The Kalman-Takens results are compared with a parametric forecasting approach of an adaptive
509 unscented Kalman filtering (AUKF) as well as against in-situ groundwater and soil moisture
510 measurements. The results prove a high capability of the Kalman-Takens for improving state
511 estimates, largely comparable to the AUKF performance and as such, both provide efficient
512 methods for assimilating GRACE TWS data. Results indicate that smaller RMSE (46.96 mm)
513 and higher NSE (0.82) values are obtained from the application of the Kalman-Takens method
514 in comparison to the open-loop run (69.40 mm RMSE and 0.58 NSE). Although AUKF per-
515 forms slightly better in some cases, e.g., $\sim 3\%$ higher improvement for groundwater estimates,
516 which is expected since AUKF takes advantage of the full knowledge of the model while the
517 non-parametric filter uses only the short noisy training data set from which to learn the dy-
518 namics, in all cases considered, the Kalman-Takens results are generally very close to those
519 of AUKF. The data-driven approach also increases the NSE values between the estimated soil
520 moisture variations and the OzNet in-situ measurements for all soil layers (11.83% on average)
521 as compared to AUKF (13.77% on average). The proposed approach also reduces estimation
522 complexities by using the local proxy model. The Kalman-Takens filter performs more efficient
523 (~ 8 times faster) in terms of computational cost, which is very important to deal with a grow-
524 ing amount of data sets in high dimensional systems. This contribution, to the best of the

525 authors' knowledge, is the first effort in using the data-driven approach in hydrological studies
526 with complex state observation transition systems. Further research should be undertaken to
527 investigate the Kalman-Takens filter in different hydrological applications and also to explore
528 its capability in dealing with multiple satellite products.

529 **6. Acknowledgement**

530 We would like to thank Tyrus Berry and Timothy Sauer for their valuable help
531 in this study. M. Khaki is grateful for the research grant of Curtin International Post-
532 graduate Research Scholarships (CIPRS)/ORD Scholarship provided by Curtin Univer-
533 sity (Australia). F. Hamilton is supported by National Science Foundation grant No.
534 RTG/DMS-1246991. This work is a TIGeR publication. The GRACE data are ac-
535 quired from the ITSG-Grace2014 gravity field model (Mayer-Gürr et al., 2014). In-situ
536 groundwater and soil moisture measurements are obtained from the New South Wales Gov-
537 ernment (NSW; <http://waterinfo.nsw.gov.au/pinneena/gw.shtml>) and the OzNet network
538 (<http://www.oznet.org.au/>), respectively. Meteorological forcing data are provided by Prince-
539 ton University (<http://hydrology.princeton.edu>). Other data used in this study can be found
540 at DOI: 10.6084/m9.figshare.5942548. A more detailed discussion of the results can be found
541 in the supporting information (Huffman et al., 2007; Mu et al., 2011).

542 **References**

- 543 Alsdorf, D.E., Rodriguez, E., Lettenmaier, D.P., (2007). Measuring surface water from space,
544 Rev. Geophys., 45, RG2002, <http://dx.doi.org/10.1029/2006RG000197>.
- 545 Andreadis, K.M., Clark, E.A., Lettenmaier, D.P., Alsdorf, D.E., (2007). Prospects for river dis-
546 charge and depth estimation through assimilation of swathaltimetry into a raster-based hydro-
547 dynamics model. Geophysical Research Letters 34: <http://dx.doi.org/10.1029/2007GL02972>.
- 548 Arnold, H., Moroz, I., Palmer, T., (2013). Stochastic Parametrizations and Model Uncertainty
549 in the Lorenz '96 System, Phil. Trans. R. Soc. A 371, 20110479.
- 550 Awwad, H.M., Valds, J.B., Restrepo, P.J., (1994). Streamflow forecasting for Han River basin,
551 Korea. J. Water Resour. Plann. Manage., 120, 651673.

552 Bennett, A.F., (2002); Inverse Modeling of the Ocean and Atmosphere, 234 pp., Cambridge
553 Univ. Press, New York.

554 Berry, T., Sauer, T., (2013). Adaptive ensemble Kalman filtering of non-linear, Tel-
555 lus A: Dynamic Meteorology and Oceanography, Volume 65, Issue 1, Article: 20331,
556 <http://dx.doi.org/10.3402/tellusa.v65i0.20331>.

557 Berry, T., Harlim, J., (2016). Variable Bandwidth Diffusion Kernels, Appl. Comput. Harmon.
558 Anal., 40, 68.

559 Boening, C., Willis, J.K., Landerer, F.W., Nerem, R.S., Fasullo, J., (2012). The
560 2011 La Nia: so strong, the oceans fell. Geophys. Res. Lett. 39, L19602.
561 <http://dx.doi.org/10.1029/2012GL053055>.

562 BoM, (2010). Australian Rainfall Patterns During El Nio Events. Bureau of Meteorology. Ac-
563 cessed at <http://www.bom.gov.au/climate/enso/ninocomp.shtml>.

564 Botterill, L.C., (2003). Uncertain Climate: The Recent History of Drought Policy in Aus-
565 tralia. Australian Journal of Politics & History, 49: 6174, [http://dx.doi.org/10.1111/1467-](http://dx.doi.org/10.1111/1467-8497.00281)
566 [8497.00281](http://dx.doi.org/10.1111/1467-8497.00281).

567 Bras, R.L., Restrepo-Posada, P., (1980). Real time automatic parameter calibration in concep-
568 tual runoff forecasting models. Proc. Third Int. Symp. on Stochastic Hydraulics, 6170.

569 Brocca, L., Melone, F., Moramarco, T., Wagner, W., Naeimi, V., Bartalis, Z., Hasenauer, S.,
570 (2010). Improving runoff prediction through the assimilation of the ASCAT soil moisture
571 product, Hydrol. Earth Syst. Sci., 14, 18811893, [http://dx.doi.org/10.5194/hess-14-1881-](http://dx.doi.org/10.5194/hess-14-1881-2010)
572 [2010](http://dx.doi.org/10.5194/hess-14-1881-2010).

573 Calvet, J.-C., Noilhan, J., Bessemoulin, P., (1998). Retrieving root-zone soil moisture from sur-
574 face soil moisture of temperature estimates: A feasibility study based on field measurements.
575 J. Appl. Meteor., 37, 371386.

576 Cheng, M.K., Tapley, B.D., (2004). Variations in the Earth's oblateness during
577 the past 28 years. Journal of Geophysical Research, Solid Earth, 109, B09402.
578 <http://dx.doi.org/10.1029/2004JB003028>.

579 Chiew, F.H.S., Stewardson, M.J., McMahon, T.A., (1993). Comparison of six rainfall-runoff
580 modelling approaches, *J. Hydrol.*, 147, 136.

581 Christiansen, L., Krogh, P.E., Bauer-Gottwein, P., Andersen, O.B., Leirio, S., Binning, P.J.,
582 Rosbjerg, D., (2007). Local to regional hydrological model calibration for the Okavango
583 River Basin from In-situ and space borne gravity observations. Proceedings of 2nd Space for
584 Hydrology Workshop, Geneva, Switzerland, 12-14.

585 Coumou, D., Rahmstorf, S., (2012). A decade of weather extremes *Nat. Clim. Change*, 2 (7),
586 pp. 16.

587 CSIRO, BoM, (2014). State of the Climate 2014. CSIRO and Bureau of Meteorology, Melbourne.

588 CSIRO, BoM, (2015). Climate change in Australia: Projections for Australia's NRM regions.
589 Technical Report, 216pp.

590 De Lannoy, G., Pauwels, V.R.N., Houser, P.R., Verhoest, N.E.C., Gish, T., (2007). Repre-
591 sentativeness of point soil moisture observations, upscaling and assimilation. IUGG General
592 Assembly, Perugia Italy, Session HS2004, July 2-13.

593 De Lannoy, G.J.M., Reichle, R.H., Houser, P.R., Pauwels, V.R.N., Verhoes, N.E.C., (2007).
594 Correcting for forecast bias in soil moisture assimilation with the ensemble Kalman filter.
595 *Water Resour. Res.* 43, W09410, <http://dx.doi.org/10.1029/2006WR00544>.

596 De Lannoy, G.J.M., Houser, P.R., Pauwels, V.R.N., Verhoest, N.E., (2009). Assessment of model
597 uncertainty for soil moisture through ensemble verification. *J. Geophys. Res.* 111, D10101,
598 <http://dx.doi.org/10.1029/2005JD006367>

599 De Lannoy, G.J.M., de Rosnay, P., Reichle, R.H., (2015). Soil Moisture Data Assimilation. In:
600 Duan Q., Pappenberger F., Thielen J., Wood A., Cloke H., Schaake J. (eds) Handbook of
601 Hydrometeorological Ensemble Forecasting. Springer, Berlin, Heidelberg.

602 DFAT (Department of Foreign Affairs and Trade) (2014). DFAT Annual Report, DFAT, Can-
603 berra.

604 Döll, P., Kaspar, F., Lehner, B., (2003). A global hydrological model for deriving water avail-
605 ability indicators: model tuning and validation, *J. Hydrol.*, 270, 105134.

- 606 Dreano, D., Mallick, B., Hoteit, I., (2015). Filtering remotely sensed chlorophyll concentrations
607 in the Red Sea using a spacetime covariance model and a Kalman filter, *Spatial Statistics*,
608 Volume 13, Pages 1-20, ISSN 2211-6753, <http://dx.doi.org/10.1016/j.spasta.2015.04.002>.
- 609 Entekhabi, D., Nakamura, H., Njoku, E.G., (1994). Solving the inverse problem for soil mois-
610 ture and temperature profiles by sequential assimilation of multifrequency remotely senses
611 observations. *IEEE Trans. Geosci. Remote Sens.*, 32, 438448.
- 612 Eicker, A., Schumacher, M., Kusche, J., Dll, P., Mller-Schmied, H., (2014). Calibration/data
613 assimilation approach for integrating GRACE data into the WaterGAP global hydrology
614 model (WGHM) using an ensemble Kalman filter: first results, *SurvGeophys*, 35(6):12851309.
615 <http://dx.doi.org/10.1007/s10712-014-9309-8>.
- 616 Elbern, H., Schmidt, H., (2001). Ozone episode analysis by fourdimensional variational chem-
617 istry data assimilation, *J. Geophys. Res.*, 106, 35693590.
- 618 Famiglietti, J.S., Ryu, D., Berg, A.A., Rodell, M., Jackson, T.J., (2008). Field ob-
619 servations of soil moisture variability across scales, *Water Resour. Res.*, 44, W01423,
620 <http://dx.doi.org/10.1029/2006WR005804>.
- 621 Forootan, E., Khandu, Awange, J., Schumacher, M., Anyah, R., van Dijk, A., Kusche, J.,
622 (2016). Quantifying the impacts of ENSO and IOD on rain gauge and remotely sensed
623 precipitation products over Australia. *Remote Sensing of Environment*, 172, Pages 50-66,
624 <http://dx.doi.org/10.1016/j.rse.2015.10.027>.
- 625 Forootan, E., Safari, A., Mostafaie, A., Schumacher, M., Delavar, M., Awange, J., (2017).
626 Large-Scale Total Water Storage and Water Flux Changes over the Arid and Semiarid Parts
627 of the Middle East from GRACE and Reanalysis Products. *Surveys in Geophysics* 38(3), pp.
628 591-615, <http://dx.doi.org/10.1007/s10712-016-9403-1>.
- 629 Giroto, M., De Lannoy, G.J.M., Reichle, R.H., Rodell, M., (2016). Assimilation of gridded
630 terrestrial water storage observations from GRACE into a land surface model, *Water Resour.*
631 *Res.*, 52, 41644183, <http://dx.doi.org/10.1002/2015WR018417>.
- 632 Giroto, M., De Lannoy, G.J.M., Reichle, R.H., Rodell, M., Draper, C., Bhanja, S.N.,
633 Mukherjee, A., (2017). Benefits and pitfalls of GRACE data assimilation: A case

634 study of terrestrial water storage depletion in India, *Geophys. Res. Lett.*, 44, 41074115,
635 <http://dx.doi.org/10.1002/2017GL072994>.

636 Giustarini, L., Matgen, P., Hostache, R., Montanari, M., Plaza, D., Pauwels, V.R.N., De Lan-
637 noy, G.J.M., De Keyser, R., Pfister, L., Hoffmann, L., Savenije, H.H.G., (2011). Assimilating
638 SAR-derived water level data into a hydraulic model: a case study, *Hydrol. Earth Syst. Sci.*,
639 15, 23492365, <http://dx.doi.org/10.5194/hess-15-2349-2011>.

640 Hamilton, F., Berry, T., Sauer, T., (2015), Predicting Chaotic Time Series with a Partial
641 Model, *Phys. Rev. E* 92, 010902.

642 Hamilton, F., Berry, T., Sauer, T., (2016). Ensemble Kalman Filtering without a Model, *Phys.*
643 *Rev. X* 6, 011021, Vol. 6, Iss. 1, <http://dx.doi.org/10.1103/PhysRevX.6.011021>.

644 Hamilton, F., Berry, T., Sauer, T., (2017). Kalman-Takens filtering in the presence of dynamical
645 noise, *To appear, Eur. Phys. J: ST*.

646 Harris, I.C., (2008). Climatic Research Unit (CRU) time-series datasets of variations in
647 climate with variations in other phenomena. NCAS British Atmospheric Data Cen-
648 tre, date of citation, University of East Anglia Climatic Research Unit; Jones, P.D.,
649 <http://catalogue.ceda.ac.uk/uuid/3f894480cc48e1cbc29a5ee12d8542d>.

650 Hersbach, H., Stoffelen, A., De Haan, S., (2007). An Improved C-Band Scatterometer Ocean
651 Geophysical Model Function: CMOD5, *J. Geophys. Res. Oceans* 112, C03006.

652 Hoteit, I., Pham, D.T., Blum, J., (2002). A simplified reducedorder kalman filtering and appli-
653 cation to altimetric data assimilation in tropical Pacific. *J. Mar. Syst.*, 36, 101127.

654 Hoteit, I., Luo, X., Pham, D.T., (2012). Particle Kalman Filtering: A Nonlinear Bayesian
655 Framework for Ensemble Kalman Filters, *Monthly Weather Review*, 140:2, 528-542.

656 Huang, S., Kumar, R., Flrke, M., Yang T., Hundecha, Y., Kraft, P., Gao, C., Gelfan, A., Liersch,
657 S., Lobanova, A., Strauch, M., Ogtrop, F.V., Reinhardt, J., Haberlandt, U., Krysanova, V.,
658 (2016). Evaluation of an ensemble of regional hydrological models in 12 large-scale river basins
659 worldwide. *Clim Chang.* <http://dx.doi.org/10.1007/s10584-016-1841-8>.

660 Huffman, G.J., Adler, R.F., Bolvin, D.T., Gu, G., Nelkin, E.J., Bowman, K.P., Hong, Y.,
661 Stocker, E.F., Wolff, D.B., (2007). The TRMM Multi-satellite Precipitation Analysis: Quasi-

662 Global, Multi-Year, Combined-Sensor Precipitation Estimates at Fine Scale. *J. Hydrometeor.*,
663 8(1), 38-55.

664 Huntington, T.G., (2006). Evidence for intensification of the global water cycle: Review and
665 synthesis, *J. Hydrol.*,319(14), 8395, <http://dx.doi.org/10.1016/j.jhydrol.2005.07.003>.

666 Irmak, A., Kamble, B., (2009). Evapotranspiration data assimilation with genetic algorithms
667 and SWAP model for on-demand irrigation. *Irrigation Science*, 28(1): 101112.

668 Julier, S.J., Uhlmann, J.K., (1997). A New Extension of the Kalman Filter to Nonlinear Sys-
669 tems. In *Proc. of AeroSense: The 11th Int. Symp. on Aerospace/Defence Sensing, Simulation*
670 *and Controls*.

671 Julier, S., Uhlmann, J., Durrant-Whyte, H.F., (2000). A new method for the nonlinear trans-
672 formation of means and covariances in filters and estimators, *IEEE Trans. Automat. Control*
673 45, 477-482.

674 Julier, S.J. and Uhlmann, J.K., (2004). Unscented filtering and nonlinear estimation, *Proc.*
675 *IEEE* 92, 401-422.

676 Kalnay, E., (2003). *Atmospheric modelling, data assimilation and predictability*, Cam-
677 bridge University Press. pp. xxii 341. ISBNs 0 521 79179 0, 0 521 79629 6,
678 <http://dx.doi.org/10.1256/00359000360683511>.

679 Kiem, A.S., Johnson, F., Westra, S., van Dijk, A., Evans, J.P., O'Donnell, A., Rouil-
680 lard, A., Barr, C., Tyler, J., Thyer, M., Jakob, D., Woldemeskel, F., Sivakumar,
681 B., Mehrotra, R., (2016). Natural hazards in Australia: droughts. *Clim. Change*.
682 <http://dx.doi.org/10.1007/s10584-016-1798-7>.

683 Khaki, M., Hoteit, I., Kuhn, M., Awange, J., Forootan, E., van Dijk, A.I.J.M., Schumacher,
684 M., Pattiaratchi, C., (2017a). Assessing sequential data assimilation techniques for integrating
685 GRACE data into a hydrological model, *Advances in Water Resources*, Volume 107, Pages
686 301-316, ISSN 0309-1708, <http://dx.doi.org/10.1016/j.advwatres.2017.07.001>.

687 Khaki, M., Schumacher, M., J., Forootan, Kuhn, M., Awange, E., van Dijk, A.I.J.M., (2017b).
688 Accounting for Spatial Correlation Errors in the Assimilation of GRACE into Hydrological
689 Models through localization, *Advances in Water Resources*, Available online 1 August 2017,
690 ISSN 0309-1708, <https://doi.org/10.1016/j.advwatres.2017.07.024>.

691 Khaki, M., Ait-El-Fquih, B., Hoteit, I., Forootan, E., Awange, J., Kuhn, M., (2017c). A two-
692 update ensemble Kalman filter for land hydrological data assimilation with an uncertain
693 constraint, In *Journal of Hydrology*, Volume 555, 2017, Pages 447-462, ISSN 0022-1694,
694 <https://doi.org/10.1016/j.jhydrol.2017.10.032>.

695 Khaki, M., Forootan, E., Kuhn, M., Awange, J., Papa, F., Shum, C.K., (2018a). A Study of
696 Bangladesh's Sub-surface Water Storages Using Satellite Products and Data Assimilation
697 Scheme, accepted in *Advances in Water Resources*.

698 Khaki, M., Forootan, E., Kuhn, M., Awange, J., van Dijk, A.I.J.M., Schumacher, M., Sharifi,
699 M.A., (2018b). Determining Water Storage Depletion within Iran by Assimilating GRACE
700 data into the W3RA Hydrological Model, *Advances in Water Resources*, 114:1-18,

701 Khaki, M., Forootan, E., Kuhn, M., Awange, J., Longuevergne, L., Wada, W., (2018c). Ef-
702 ficient Basin Scale Filtering of GRACE Satellite Products, In *Remote Sensing of Environ-*
703 *ment*, Volume 204, Pages 76-93, ISSN 0034-4257, <https://doi.org/10.1016/j.rse.2017.10.040>.
704 <https://doi.org/10.1016/j.advwatres.2018.02.008>.

705 Kumar, S.V., Reichle, R.H., Koster, R.D., Crow, W.T., Peters-Lidard, C.D., (2009). Role of
706 subsurface physics in the assimilation of surface soil moisture observations. *J. Hydromet.* 10
707 (6), 15341547. <http://dx.doi.org/10.1175/2009JHM1134.1>.

708 Kumar, S.V., Peters-Lidard, C.D., Santanello, J.A., Reichle, R.H., Draper, C.S., Koster,
709 R.D., Nearing, G., Jasinski, M.F., (2015). Evaluating the utility of satellite soil mois-
710 ture retrievals over irrigated areas and the ability of land data assimilation methods to
711 correct for unmodeled processes, *Hydrology and Earth System Sciences*, 19, 4463-4478,
712 <http://dx.doi.org/10.5194/hess-19-4463-2015>.

713 Kumar, S., Zaitchik, B., Peters-Lidard, C., Rodell, M., Reichle, R., Li, B., Jasinski, M.,
714 Mocko, D., (2016). Assimilation of Gridded GRACE Terrestrial Water Storage Estimates
715 in the North American Land Data Assimilation System. *J. Hydrometeor.*, 17, 19511972,
716 <http://dx.doi.org/10.1175/JHM-D-15-0157.1>.

717 Kusche, J., Schmidt R., Petrovic, S., Rietbroek, R., (2009). Decorrelated GRACE time-variable
718 gravity solutions by GFZ and their validation using a hydrological model, *Journal of Geodesy*,
719 DOI 10.1007/s00190-009-0308-3.

720 Lahoz, W.A., Geer, A.J., Bekki, S., Bormann, N., Ceccherini, S., Elbern, H., Errera, Q., Eskes,
721 H.J., Fonteyn, D., Jackson, D.R., Khattatov, B., (2007). The Assimilation of Envisat data
722 (ASSET) project, *Atmos. Chem. Phys.*, 7, 1773 - 1796.

723 Lagergren, J., Reeder, A., Hamilton, F., Smith, R.C., Flores, K.B., (2018). Forecasting and
724 Uncertainty Quantification Using a Hybrid of Mechanistic and Non-mechanistic Models for
725 an Age-Structured Population Model, *Bull Math Biol*, [https://doi.org/10.1007/s11538-018-](https://doi.org/10.1007/s11538-018-0421-7)
726 0421-7.

727 Botterill, L.C., Fisher, M., (2012). *Beyond Drought: People, Policy and Perspectives*, CSIRO
728 Publishing, Melbourne, DAFF (Department of Agriculture, Fisheries and Forestry), Drought
729 and Natural Disaster Declaration: 12 September. Queensland Government. Accessed at
730 <https://www.longpaddock.qld.gov.au/queenslanddroughtmonitor/queenslanddroughtreport/>.

731 LeBlanc, M., Tweed, S., Van Dijk, A., Timbal, B., (2012). A review of historic and future
732 hydrological changes in the Murray Darling Basin. *Global Planetary Change* (8081): 226246.

733 Lee, H., Seo, D.-J., Koren, V., (2011). Assimilation of streamflow and in situ soil mois-
734 ture data into operational distributed hydrologic models: Effects of uncertainties in
735 the data and initial model soil moisture states, *Adv. Water Resour.*, 34(12), 15971615,
736 <http://dx.doi.org/10.1016/j.advwatres.2011.08.012>.

737 Lguensat, R., Tandeo, P., Ailliot, P., Pulido, M., Fablet, R., (2017). The Analog Data Assimi-
738 lation. *Mon. Wea. Rev.*, <https://doi.org/10.1175/MWR-D-16-0441.1>.

739 Li, Y., Ryu, D., Western, A.W., Wang, Q.J., (2015). Assimilation of stream discharge for flood
740 forecasting: Updating a semidistributed model with an integrated data assimilation scheme,
741 *Water Resour. Res.*, 51, 32383258, <http://dx.doi.org/10.1002/2014WR016667>.

742 Lievens, H., Kumar, S., Al Bitar, A., De Lannoy, G.J.M., Drusch, M., Dumedah, G., Hendricks
743 Franssen, H.J., Kerr, Y.H., Martens, B., Pan, M., Roundy, J.K., Vereecken, H., Walker, J.P.,
744 Wood, E.F., Verhoest, N.E.C., Pauwels, V.R.N., (2015). SMOS soil moisture assimilation for
745 improved hydrologic simulation in the Murray Darling Basin, Australia, *Remote Sensing of*
746 *Environment*, 168(10), 146162.

747 Madsen, H., Skotner, C., (2005). Adaptive state-updating in real-time river flow forecastingA
748 combined filtering and error forecasting procedure. *J. Hydrol.*, 308, 302312.

749 Mayer-Gürr, T., Zehentner, N., Klinger, B., Kvas, A., (2014). ITSG-Grace2014: a new GRACE
750 gravity field release computed in Graz. - in: GRACE Science Team Meeting (GSTM), Pots-
751 dam am: 29.09.2014.

752 McMillan, H.K., Hreinsson, E., Clark, M.P., Singh, S.K., Zammit, C., Uddstrom, M.J., (2013).
753 Operational hydrological data assimilation with the recursive ensemble Kalman filter, *Hydrol.*
754 *Earth Syst. Sci.*, 17(1), 2138, <http://dx.doi.org/10.5194/hess-17-21-2013>.

755 Mehra, R., (1970). On the identification of variances and adaptive Kalman filtering. *IEEE*
756 *Trans. Auto. Cont.* 15, 175-184.

757 Mehra, R., (1972). Approaches to adaptive filtering. *IEEE Trans. Auto. Cont.* 17, 693-698.

758 Mercer, D., Christesen, L., Buston, M., (2007). Squandering the futureClimate change, policy
759 failure and the water crisis in Australia. *Futures* 39: 272287.

760 Montaldo, N., Albertson, J.D., Mancini, M., Kiely, G., (2001). Robust simulation of root zone
761 soil moisture with assimilation of surface soil moisture data. *Water Resour. Res.*, 37, 28892900.

762 Mu, Q., Zhao, M., Running, S.W., (2011). Improvements to a MODIS Global Terrestrial Evap-
763 otranspiration Algorithm. *Remote Sensing of Environment* 115: 1781-1800.

764 Müller Schmied, H., S. Eisner, D. Franz, M. Wattenbach, F. Portmann, M. Flrke, Dll, P.,
765 (2014). Sensitivity of simulated global-scale freshwater fluxes and storages to input data,
766 hydrological model structure, human water use and calibration, *Hydrol. Earth. Syst. Sci.*, 18,
767 35113538, <http://dx.doi.org/10.5194/hess-18-3511-2014>.

768 Neal, J., Schumann, G., Bates, P., Buytaert, W., Matgen, P., Pappenberger, F., (2009). A data
769 assimilation approach to discharge estimation from space, *Hydrol. Process.*, 23, 36413649.

770 Nicolai-Shaw, N., Hirschi, M., Mittelbach, H., Seneviratne, S.I., (2015). Spatial representative-
771 ness of soil moisture using in situ, remote sensing, and land reanalysis data, *J. Geophys. Res.*
772 *Atmos.*, 120, 99559964, <http://dx.doi.org/10.1002/2015JD023305>.

773 Orłowsky, B., Seneviratne, S.I., (2014). On the spatial representativeness of tempo-
774 ral dynamics at European weather stations, *Int. J. Climatol.*, 34(10), 31543160,
775 <http://dx.doi.org/10.1002/joc.3903>.

776 Packard, N.H., Crutchfield, J.P., Farmer, J.D., Shaw, R.S., (1980). Geometry from a Time
777 Series, *Phys. Rev. Lett.* 45, 712.

778 Palmer, T.N., (2001). A Nonlinear Dynamical Perspective on Model Error: A Proposal for
779 Non-Local Stochastic-Dynamic Parametrization in Weather and Climate Prediction Models,
780 *Q. J. R. Meteorol. Soc.* 127, 279.

781 Pipunic, C., Walker, P., Western, A., (2008). Assimilation of remotely sensed data for improved
782 latent and sensible heat flux prediction: A comparative synthetic study. *Remote Sensing of*
783 *Environment*, 112(4): 12951305.

784 Rasmussen, J., Madsen, H., Jensen, K.H., and Refsgaard, J.C., (2015). Data assimilation in
785 integrated hydrological modeling using ensemble Kalman filtering: evaluating the effect of
786 ensemble size and localization on filter performance, *Hydrol. Earth Syst. Sci.*, 19, 2999-3013,
787 <https://doi.org/10.5194/hess-19-2999-2015>.

788 Reager, J.T., Thomas, A.C., Sproles, E.A., Rodell, M., Beaudoin, H.K., Li, B., Famiglietti,
789 J.S., (2015). Assimilation of GRACE Terrestrial Water Storage Observations into a Land
790 Surface Model for the Assessment of Regional Flood Potential. *Remote Sens.* 2015, 7, 14663-
791 14679.

792 Reichle, R.H., McLaughlin, D.B., Entekhabi, D., (2002). Hydrologic Data Assimilation with
793 the Ensemble Kalman Filter. *Mon. Wea. Rev.* 130, 103114, [http://dx.doi.org/10.1175/1520-0493\(2002\)130;0103:HDAWTE;2.0.CO;2](http://dx.doi.org/10.1175/1520-0493(2002)130;0103:HDAWTE;2.0.CO;2).

795 Reichle, R.H., Koster, R.D., (2005). Global Assimilation of Satellite Surface Soil Moisture
796 Retrievals into the NASA Catchment Land Surface Model, *Geophys. Res. Lett.* 32, L02404.

797 Renzullo, L.J., Van Dijk, A.I.J.M., Perraud, J.M., Collins, D., Henderson, B., Jin, H., Smith,
798 A.B., McJannet, D.L., (2014). Continental satellite soil moisture data assimilation im-
799 proves root-zone moisture analysis for water resources assessment. *J. Hydrol.*, 519, 27472762.
800 <http://dx.doi.org/10.1016/j.jhydrol.2014.08.008>.

801 Rodell, M., Chen, J., Kato, H., Famiglietti, J.S., Nigro, J., Wilson, C.R., (2007). Estimating
802 groundwater storage changes in the Mississippi River basin (USA) using GRACE, *Hydrogeol.*
803 *J.*, 15, 159166.

- 804 Sauer, T., Yorke, J., Casdagli, M., (1991). Embedology, *J. Stat. Phys.* 65, 579.
- 805 Sauer, T., (2004). Reconstruction of Shared Nonlinear Dynamics in a Network, *Phys. Rev. Lett.*
806 93, 198701.
- 807 Schumacher, M., Kusche, J., Dll, P., (2016). A systematic impact assessment of GRACE
808 error correlation on data assimilation in hydrological models, *Journal of Geodesy*,
809 <http://dx.doi.org/10.1007/s00190-016-0892-y>.
- 810 Schumacher, M., Forootan, E., van Dijk, A.I.J.M., Mller Schmied, H., Crosbie, R.S., Kusche,
811 J., Dll, P., (2018). Improving drought simulations within the Murray-Darling Basin by
812 combined calibration/assimilation of GRACE data into the WaterGAP Global Hydrology
813 Model, In *Remote Sensing of Environment*, Volume 204, Pages 212-228, ISSN 0034-4257,
814 <https://doi.org/10.1016/j.rse.2017.10.029>.
- 815 Schunk, R.W., Scherliess, L., Sojka, J.J., Thompson, D.C., (2004). USU global ionospheric data
816 assimilation models, *Atmospheric and Environmental Remote Sensing Data Processing and*
817 *Utilization: an End-to-End System Perspective*, (ed. H.-L. A. Huang and H. J. Bloom), *Proc.*
818 *of SPIE*, 5548, <http://dx.doi.org/10.1117/12.562448>, 327-336.
- 819 Schuurmans, M., Troch A., Veldhuizen, A., et al., (2003). Assimilation of remotely sensed latent
820 heat flux in a distributed hydrological model. *Advances in Water Resources*, 26(2): 151159.
- 821 Seo, D.J., Koren, V., Cajina, N., (2003). Real-time variational assimilation of hydrologic and hy-
822 drometeorological data into operational hydrologic forecasting. *J. Hydrometeorol.*, 4, 627641.
- 823 Seoane, L., Ramillien, G., Frappart, F., Leblanc, M., (2013). Regional GRACE-based estimates
824 of water mass variations over Australia: validation and interpretation, *Hydrol. Earth Syst.*
825 *Sci.*, 17, 4925-4939, <http://dx.doi.org/10.5194/hess-17-4925-2013>.
- 826 Sheffield, J., Goteti, G., Wood, E. F., (2006). Development of a 50-yearhigh-resolution global
827 dataset of meteorological forcings for land surfacemodeling, *J. Clim.*, 19(13), 30883111.
- 828 Simon, D., (2006). *Optimal state estimation: Kalman, H_∞ , and nonlinear approaches*, John
829 Wiley and Sons.
- 830 Smith, P.J., Dance, S.L., Nichols, N.K., (2011). A hybrid data assimilation scheme
831 for model parameter estimation: Application to morphodynamic modelling, *Comput-*

832 ers and Fluids, Volume 46, Issue 1, July 2011, Pages 436-441, ISSN 0045-7930,
833 <http://dx.doi.org/10.1016/j.compfluid.2011.01.010>.

834 Song, Q., He, Y., (2009). Adaptive unscented Kalman filter for estimation of modelling errors for
835 helicopter, IEEE International Conference on Robotics and Biomimetics (ROBIO), Guilin,
836 2009, pp. 2463-2467, <http://dx.doi.org/10.1109/ROBIO.2009.5420406>.

837 Swenson, S., Chambers, D., Wahr, J., (2008). Estimating geocentervariations from a combi-
838 nation of GRACE and ocean model output. Journal of Geophysical research, 113, B08410,
839 <http://dx.doi.org/10.1029/2007JB005338>.

840 Takens, F., (1981). Dynamical Systems and Turbulence, Warwick 1980, Lect. Notes Math. 898,
841 366.

842 Tandeo, P., Coauthors, (2015). Combining analog method and ensemble data assimilation:
843 application to the lorenz-63 chaotic system. Machine Learning and Data Mining Approaches
844 to Climate Science, Springer, 312.

845 Tangdamrongsub, N., Steele-Dunne, S.C., Gunter, B.C., Ditmar, P.G., and Weerts, A.H.,
846 (2015). Data assimilation of GRACE terrestrial water storage estimates into a regional
847 hydrological model of the Rhine River basin, Hydrol. Earth Syst. Sci., 19, 2079-2100,
848 <http://dx.doi.org/10.5194/hess-19-2079-2015>.

849 Tardif, R., Hakim, G.J., Snyder, C., (2015). Coupled atmosphereocean data assimila-
850 tion experiments with a low-order model and CMIP5 model data, Clim Dyn 45: 1415.
851 <https://doi.org/10.1007/s00382-014-2390-3>.

852 Terejanu, G.A., (2009). Unscented Kalman filter tutorial, Workshop on Large-Scale Quantifi-
853 cation of Uncertainty, Sandia National Laboratories, pp. 16.

854 Thomas, A.C., Reager, J.T., Famiglietti, J.S., Rodell, M., (2014). A GRACE-based water
855 storage deficit approach for hydrological drought characterization. Geophys. Res. Lett. 41,
856 15371545.

857 Tian, S., Tregoning, P., Renzullo, L.J., van Dijk, A.I.J.M., Walker, J.P., Pauwels, V.R.N.,
858 Allgeyer, S., (2017). Improved water balance component estimates through joint assimila-
859 tion of GRACE water storage and SMOS soil moisture retrievals, Water Resour. Res., 53,
860 <http://dx.doi.org/10.1002/2016WR019641>.

861 Ummenhofer, C.C., England, M.H., McIntosh, P.C., Meyers, G.A., Pook, M.J., Risbey, J.S.,
862 Sen Gupta, A., Taschetto, A.S., (2009). What causes southeast Australia's worst droughts?
863 *Geophys. Res. Lett.* 36, L04706. <http://dx.doi.org/10.1029/2008GL036801>.

864 Van der Merwe, R., (2004). Sigma-Point Kalman Filters for probability inference in dynamic
865 state-space models, PhD Thesis, Oregon Health and Science University.

866 van Dijk, A.I.J.M., (2010). The Australian Water Resources Assessment System: Technical
867 Report 3, Landscape model (version 0.5) Technical Description, CSIRO: Water for a Healthy
868 Country National Research Flagship.

869 van Dijk, A.I.J.M., Renzullo, L.J., and Rodell, M., (2011). Use of Gravity Recovery and
870 Climate Experiment terrestrial water storage retrievals to evaluate model estimates by
871 the Australian water resources assessment system, *Water Resour. Res.*, 47, W11524,
872 <http://dx.doi.org/10.1029/2011WR010714>.

873 van Dijk, A.I.J.M., Pea-Arancibia, J.L., Wood, E.F., Sheffield, J., Beck, H.E., (2013). Global
874 analysis of seasonal streamflow predictability using an ensemble prediction system and
875 observations from 6192 small catchments worldwide, *Water Resour. Res.*, 49, 27292746,
876 <http://dx.doi.org/10.1002/wrcr.20251>.

877 van Dijk, A.I.J.M., Renzullo, L.J., Wada, Y., Tregoning, P., (2014). A global water cycle reanal-
878 ysis (20032012) merging satellite gravimetry and altimetry observations with a hydrological
879 multi-model ensemble. *Hydrol Earth Syst Sci* 18:29552973. [http://dx.doi.org/10.5194/hess-](http://dx.doi.org/10.5194/hess-18-2955-2014)
880 [18-2955-2014](http://dx.doi.org/10.5194/hess-18-2955-2014).

881 Vrugt, J.A., Diks, C.G., Gupta, H.V., Bouten, W., Verstraten, J.M., (2005). Im-
882 proved treatment of uncertainty in hydrologic modeling: Combining the strengths
883 of global optimization and data assimilation. *Water Resour. Res.*, 41, W01017,
884 <http://dx.doi.org/10.1029/2004WR003059>.

885 Vrugt, J.A., Gupta, H.V., Nualain, B.O., (2006). Real-time data assimilation
886 for operational ensemble streamflow forecasting, *J. Hydrometeorol.*, 7(3), 548565,
887 <http://dx.doi.org/10.1175/JHM504.1>.

888 Vrugt, J.A., ter Braak, C.J.F., Diks, C.G.H., Schoups, G., (2013). Advancing hydrologic
889 data assimilation using particle Markov chain Monte Carlo simulation: theory, concepts

890 and applications, *Advances in Water Resources*, Anniversary Issue - 35 Years, 51, 457-478,
891 <http://dx.doi.org/10.1016/j.advwatres.2012.04.002>.

892 Wahr, J.M., Molenaar, M., Bryan, F., (1998). Time variability of the Earth's gravity field:
893 hydrological and oceanic effects and their possible detection using GRACE. *J Geophys Res*
894 108(B12):3020530229, <http://dx.doi.org/10.1029/98JB02844>.

895 Wan, E., van der Merwe, R., (2000). The unscented Kalman filter for nonlinear estima-
896 tion, *Proceedings of the IEEE 2000 Adaptive Systems for Signal Processing, Communica-*
897 *tions, and Control Symposium (Cat. No.00EX373)*, Lake Louise, Alta., 2000, pp. 153-158,
898 <http://dx.doi.org/10.1109/ASSPCC.2000.882463>.

899 Wan, E., van der Merwe, R., (2001). *The Unscented Kalman Filter*. Wiley Publishing.

900 Weerts, A.H., El Serafy, G.Y.H., (2006). Particle filtering and ensemble Kalman filtering for
901 state updating with hydrological conceptual rainfall-runoff models. *Water Resour. Res.*, 42,
902 W09403, <http://10.1029/2005WR004093>.

903 Wooldridge, S.A., Kalma, J.D., (2001). Regional-scale hydrological modelling using multiple-
904 parameter landscape zones and a quasi-distributed water balance model. *Hydrological Earth*
905 *System Sciences*. 5: 59-74.

906 Yin, J., Zhan, C., Gu, H., et al., (2014). A case study of evapotranspiration data assimilation
907 based on hydrological model. *Advances in Earth Science*, 29(9): 10751084.

908 Young, P.C., (2002). *Advances in real-time flood forecasting*. *Philos. Trans. Roy. Soc. London*,
909 360, 14331450.

910 Zaitchik, B.F., Rodell, M., Reichle, R.H., (2008). Assimilation of GRACE terrestrial water stor-
911 age data into a land surface model: results for the Mississippi River Basin. *J Hydrometeorol*
912 9(3):535548, <http://dx.doi.org/10.1175/2007JHM951.1>.

913 Zhang, Y., Bocquet, M., Mallet, V., Seigneur, C., and Baklanov, A., (2012). Real-time air
914 quality forecasting, Part I: History, techniques, and current status, *Atmos. Environ.*, 60,
915 632655.

916 Zhao, Y., Deng, X., Zhang, S., Liu, Z., Liu, C., Vecchi, G., Han, G., Wu, X., (2017). Impact of

917 an observational time window on coupled data assimilation: simulation with a simple climate
918 model, *Nonlin. Processes Geophys.*, 24, 681-694, <https://doi.org/10.5194/npg-24-681-2017>.

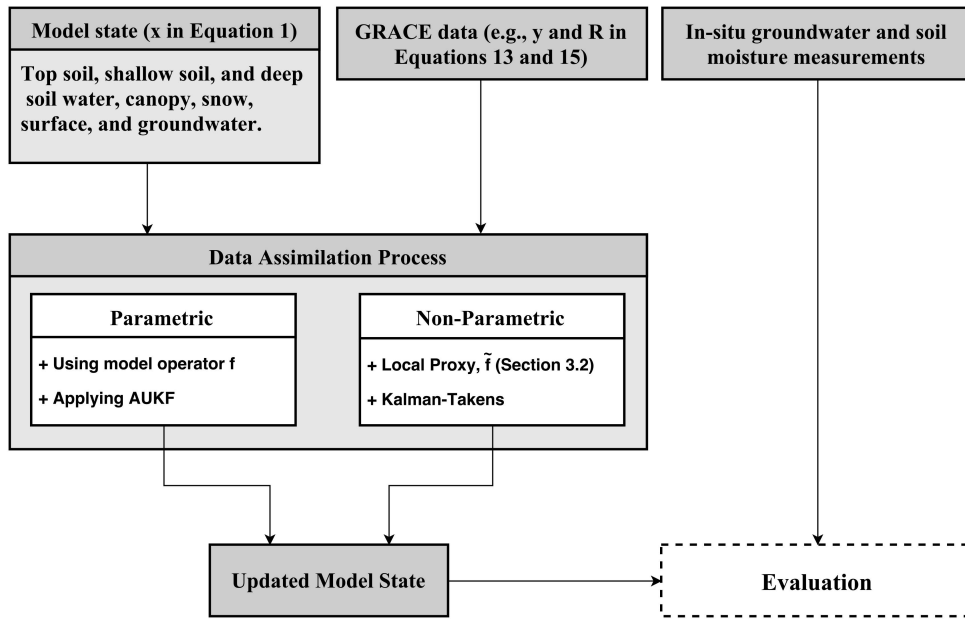


Figure 1: A schematic illustration of the data integration process implemented for this study.

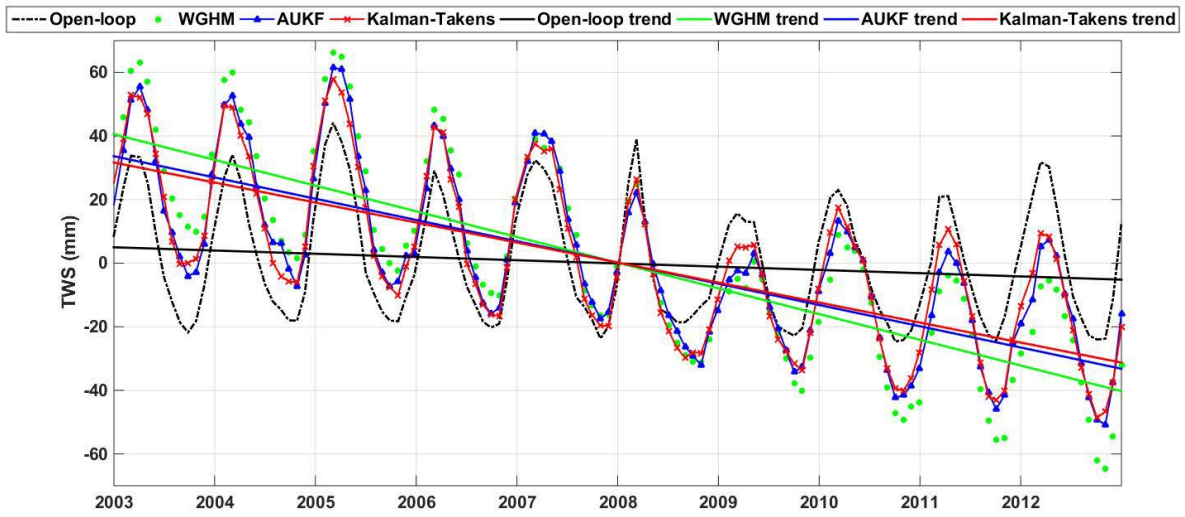


Figure 2: Average TWS variation time series over Iran from AUKF, Kalman-Takens, open-loop run, and WGHM with corresponding trend lines.

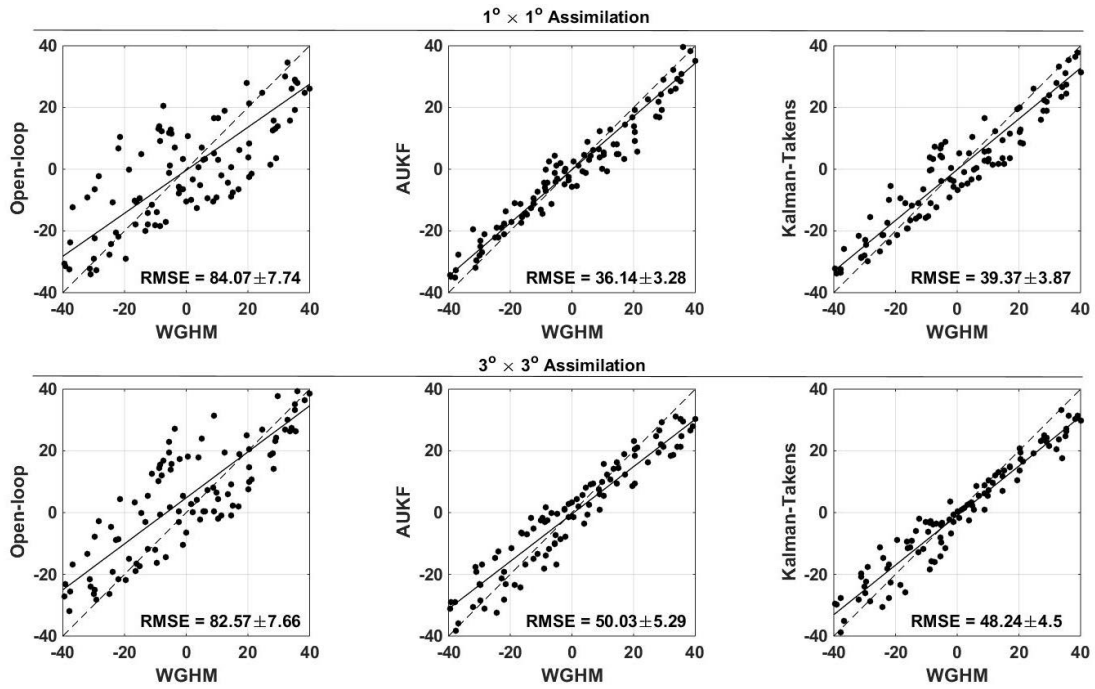


Figure 3: Scatter plots of open-loop, AUKF, and Kalman-Takens TWS estimates with respect to WGHM TWS at the two spatial resolution of $1^\circ \times 1^\circ$ and $3^\circ \times 3^\circ$. The presented average RMSE values for each method is calculated based on the original WGHM TWS (before perturbation using GRACE errors). In each sub-figure reference (dashed) and fitted (solid) lines are illustrated.

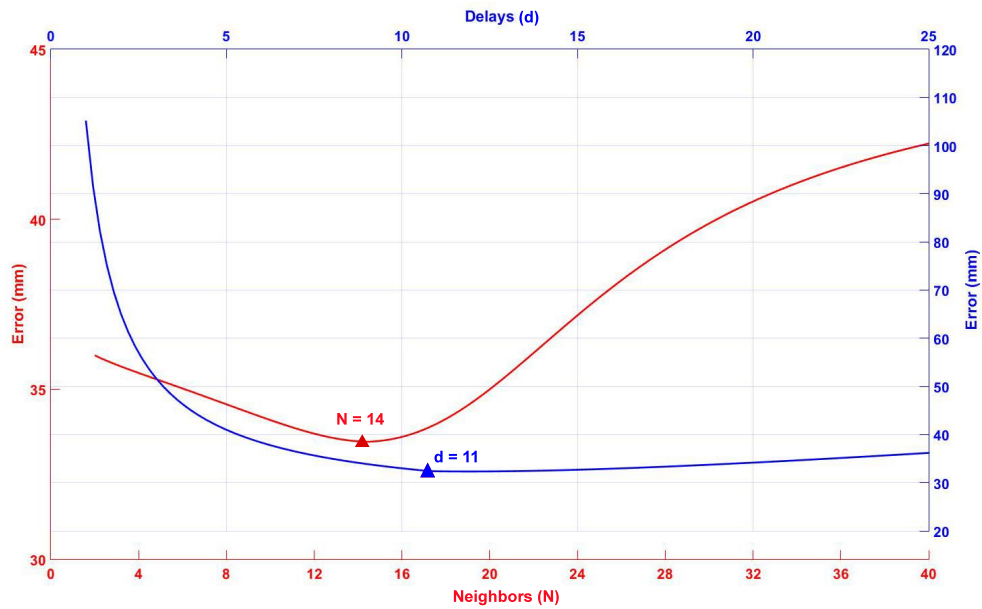


Figure 4: Estimated average errors from different scenarios considered based on the number of neighbors N and delays d . The best estimates are achieved by applying the Kalman-Takens method using $N = 14$ and $d = 11$.

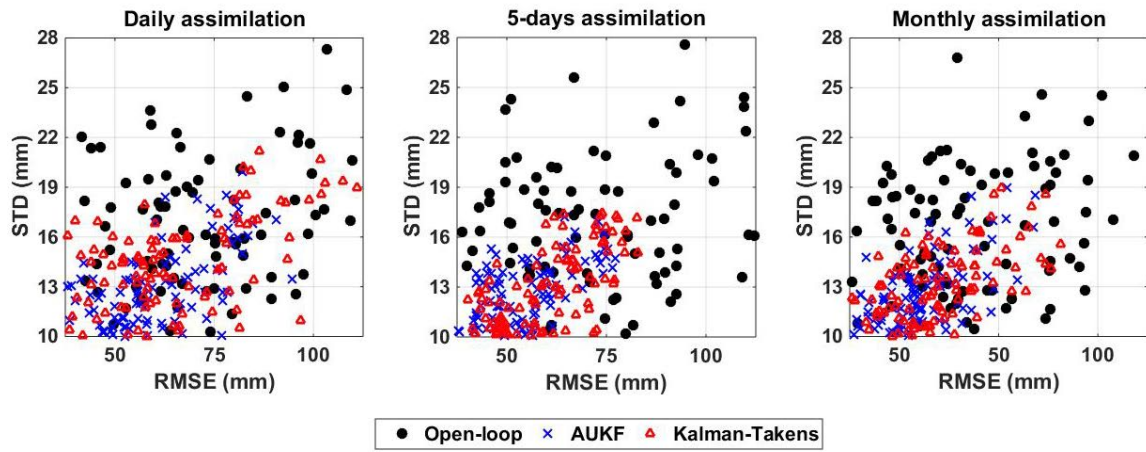


Figure 5: Average groundwater RMSE and STD of from the Kalman-Takens filter, AUKF, and open-loop run computed using groundwater in-situ measurement. The results are presented for assimilation with three different temporal scales (i.e., daily, 5-day, and monthly).

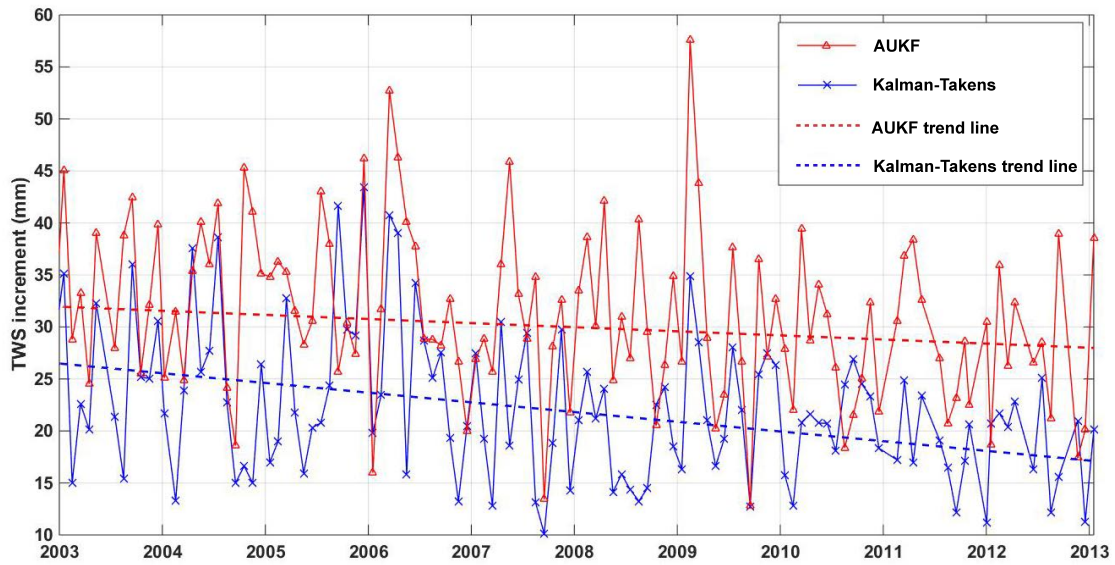


Figure 6: An average TWS increment time series of AUKF and the Kalman-Takens filter on state vectors during the process. Both methods decrease the increment as assimilation proceeds forward in time.

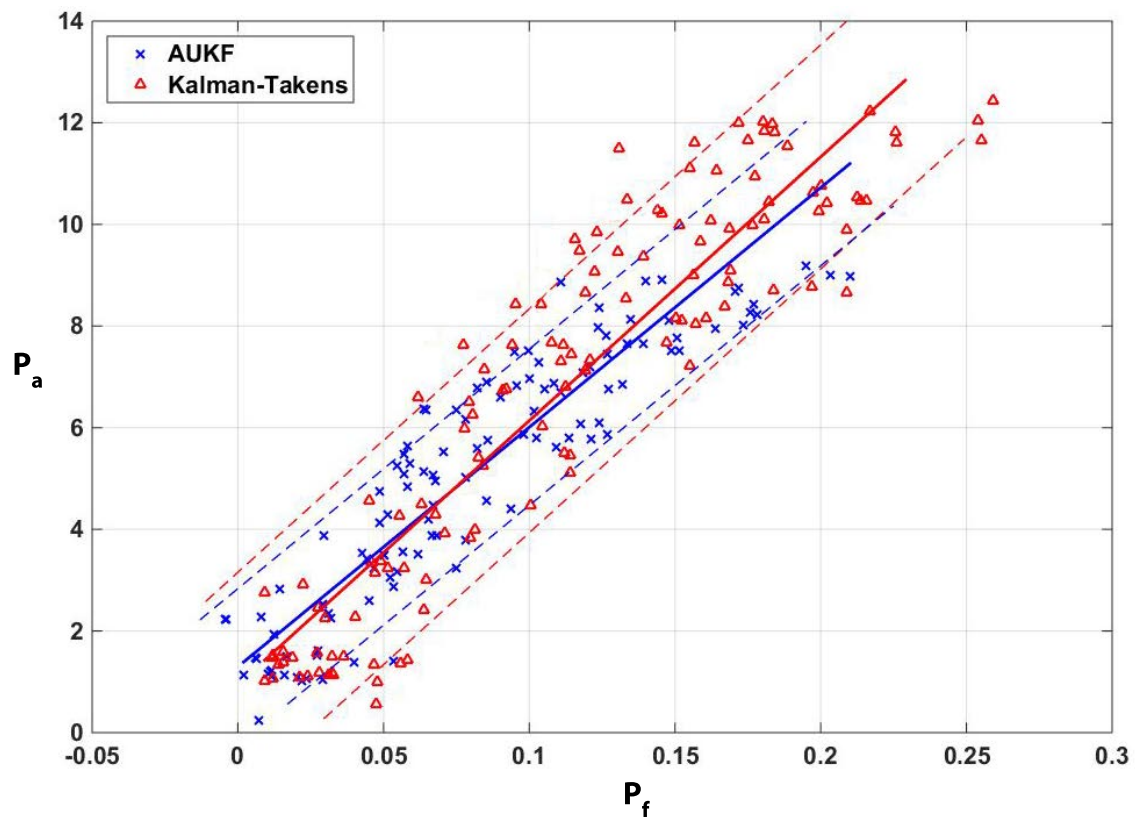


Figure 7: An average estimated covariance matrices of P_f and P_a corresponding to 95% confidence level (dashed lines) at each filtering step using the implemented filters.

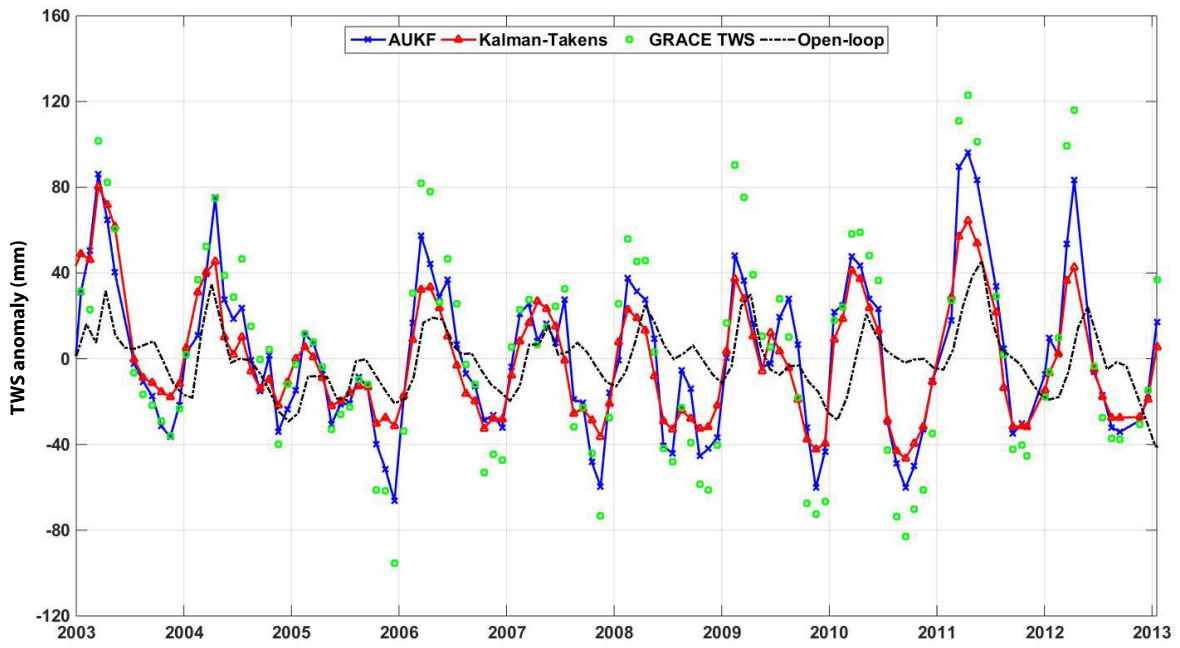


Figure 8: Spatially averaged TWS time series of filters' estimates, GRACE TWS observations, and open-loop run within Australia.

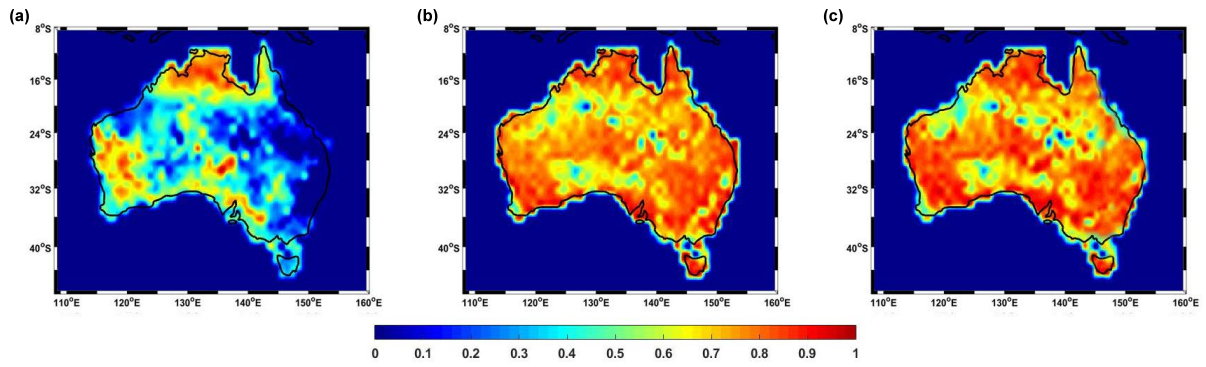


Figure 9: Spatial correlations maps between GRACE TWS and open-loop run (a), AUKF estimates (b), and the Kalman-Takens filter (c).

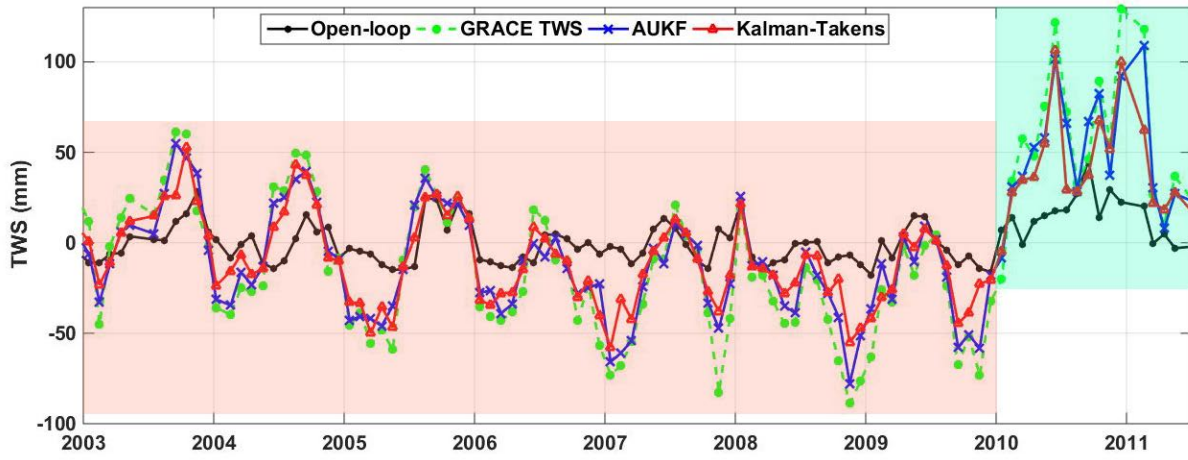


Figure 10: Average TWS variations from the data assimilation filters, open-loop run, and GRACE TWS. The red shaded area shows the Millennium Drought and blue shaded area represent a strong ENSO effect.

Table 1: Summary of statistical values derived from the implemented methods using the groundwater in-situ measurements. The reduction of the RMSE value of the AUKF and Kalman-Takens filters are calculated in relation to the RMSE of the open-loop run.

Metric	Grid-based evaluation			Basin scale evaluation		
	Open-loop	AUKF	Kalman-Takens	Open-loop	AUKF	Kalman-Takens
RMSE (<i>mm</i>)	74.57	51.28	53.61	69.40	45.16	46.96
NSE	0.51	0.77	0.75	0.58	0.82	0.81
RMSE reduction (%)	–	31.23	28.11	–	34.93	32.33

Table 2: Summary of NSE values estimated using state estimates derived from implemented methods and the soil moisture in-situ measurements at different layers. The improvements (in %) are calculated based on the increased correlation by applying the methods with respect to the open-loop run.

	Method	0-8 cm	0-30 cm	0-90 cm
	Open-loop	0.59	0.64	0.72
	AUKF	0.63	0.71	0.89
	Kalman-Takens	0.61	0.73	0.85
Improvements (%)	AUKF	6.77	10.94	23.61
	Kalman-Takens	3.39	14.06	18.05